Distorted-wave calculation of the $(p,p'\pi^+)$ reaction

R. Mehrem,* J. T. Londergan, and G. E. Walker
Department of Physics and Nuclear Theory Center, Indiana University, 2401 Milo Sampson Lane, Bloomington, Indiana 47408
(Received 23 March 1993)

The direct nuclear reaction $(N,N'\pi)$ on light nuclei is investigated using an intermediate isobar model. Cross sections for this exclusive reaction are calculated in distorted-wave approximation, for an incident nucleon of energy 300–800 MeV scattering from a closed-shell target, where the final nucleon and pion are detected in coincidence. The residual nucleus is assumed to be in a particle-hole state of arbitrary angular momentum and isospin. This reaction permits a small momentum transfer to the nucleus (1 fm^{-1}) so the nuclear structure is relatively well known. We study the dependence of these cross sections on several factors. The greatest sensitivity is to the self-energy of the intermediate meson. By considering different spin and parity nuclear final states, the nucleus is used as a spin-isospin filter allowing one to select certain amplitudes and study them independently. As an example, a detailed numerical study of the coincidence reaction on ^{16}O is carried out. Such coincidence experiments may be useful for studying various aspects of the production and propagation of mesons and isobars in nuclei.

PACS number(s): 25.40.−h

I. INTRODUCTION

The (p,π) reaction for proton-induced pion production has now been studied for over two decades [1]. Study of this reaction was motivated by a desire to understand the effects of the nuclear medium on the properties of the $\Delta(1232)$ isobar, and also to probe the high-momentum components of single-particle wave functions [2]. At the present time, only partial success can be claimed in understanding either the reaction mechanism or the nuclear response. Originally, the reaction was analyzed using the so-called "one-nucleon mechanism" [3]. This assumed that the (p,π) reaction occurred when the incident proton radiated a single pion in a process analogous to bremsstrahlung. The one-nucleon mechanism has difficulties in reproducing measured (p,π) cross sections for at least three reasons. First, experimental cross sections for (p,π^+) reactions frequently show significant population for two-particle–one-hole final nuclear states. Such states cannot be populated in the single-nucleon pion production mechanism. They could be excited by the ensuing final-state interactions between the outgoing pion and nucleus, but this excitation process clearly involves another active nucleon. Second, the (p,π^-) reaction on a nuclear target is particularly difficult to model; as in the one-nucleon approach, it requires pion single or double charge-exchange in the pion-nucleus interactions which follow the pion production event. The discovery by Jacobs *et al.* [4] that (p,π^-) cross sections leading to certain two-particle–one-hole final states were as large as some (p,π^+) transitions was particularly difficult to explain in the one-nucleon picture. Finally, in the one-nucleon mechanism the entire transferred momentum is absorbed by a single particle. Thus the production amplitude is proportional to single-particle transition densities evaluated at a very large momentum transfer, and should lead to very small cross sections. This reaction mechanism thus has difficulty giving quantitative agreement with the variety of experimental results on these reactions.

A more successful reaction mechanism has been the two-nucleon model [5], in which two active nucleons (the projectile and one target nucleon) participate. In such a model, the above objections are at least partially resolved. The two active nucleons can share the large momentum transfer, leading to larger predicted cross sections and naturally explaining the significant population of two-particle–one-hole nuclear states. Similarly, this reaction mechanism seems more natural to explain the observed (p,π^-) cross sections. However, application of these models to the substantial body of experiments has met with only partial success, and quantitative agreement with all of the data has not been possible to date.

A second type of experiment which has been widely studied is the production and propagation of the $\Delta(1232)$ isobar in nuclear reactions. For example, in intermediate-energy pion reactions with nuclei, the isobar-hole model [6–12] has proven quite successful in confronting a wide variety of data. As the Δ is a spin-isospin excitation of the nucleon in the constituent quark model, it should be a prominent feature in spin-isospin excitations initiated by baryons. As examples, studies of charge-exchange reactions like (p,n) and $(^3He,t)$ have proven very fruitful [13]. Clear evidence for isobar excitation has been observed in these reactions and we now have a semiquantitative understanding of these processes. However, significant questions still remain in our understanding of Δ-nuclear systems.

In this paper we study the $(p,p'\pi^+)$ reaction at intermediate energies. This work is motivated from several considerations. The first of these is to examine a reaction which should be dominated by Δ excitation in the kinematic region studied. Thus measurement of the final pro-

*Present address: L-412, Lawrence Livermore National Laboratory, Livermore, CA 94550.

ton and pion in coincidence can focus on processes in which a Δ is formed, propagates, and decays. In such reactions it is possible to isolate the kinematic region where the $N\pi$ pair arise from on-shell Δ formation. Thus this reaction can study processes dominated by essentially real Δ production and propagation in nuclei. Analysis of the (p,π) reaction has proven difficult because the dominant reaction process involves a pair of bound nucleons in the final state. An advantage of the $(N,N'\pi)$ reaction is that the approximation involving only a single "active" target nucleon should be rather accurate, particularly for exclusive reactions leading to one-particle–one-hole final nuclear states.

A second motive is to study pion production reactions which may involve rather favorable kinematics for understanding the associated nuclear structure. Unlike the exclusive (p,π) reaction, which is necessarily a high-momentum transfer process, it is possible for the $(N,N'\pi)$ reaction to require reasonably small nuclear momentum transfer for some geometries, while the reaction mechanism for $(N,N'\pi)$ is very similar to that previously studied in the (p,π) reaction. In other kinematic regions the $(N,N'\pi)$ process occurs at very high-momentum transfer. Therefore, study of the $(N,N'\pi)$ reaction holds the promise of disentangling some of the uncertainties inherent in the (p,π) reaction. A goal would be to produce a model capable of predicting these cross sections in the region of small nuclear momentum transfer, where the only significant uncertainty should be the reaction mechanism. Once a satisfactory fit is achieved here, one could extrapolate the model to the very high-momentum transfer regime, where the nuclear response function is largely unknown.

A third motivation for examining these reactions is the spin-isospin character of the $\Delta(1232)$ isobar. We shall show that for a closed-shell target, the spin and isospin amplitudes for the $(N,N'\pi)$ reaction leading to specific final states receive contributions only from certain of the possible amplitudes in this transition. Therefore, if one examines the excitation of particular configuration mixed one-particle–one-hole states in such a reaction, the nucleus can be used as a spin-isospin filter to study specific transitions. In this way theoretical predictions for exciting specific states (or groups of states) can be used to test the adequacy of the assumed reaction mechanism.

The organization of this paper proceeds as follows. In Sec. II we outline the assumed reaction mechanism. The $(N,N'\pi)$ reaction is calculated in the kinematic region dominated by intermediate Δ formation. It is assumed that the reaction proceeds via a single hard scattering between two active nucleons, the projectile and a nucleon in the target. This hard scattering excites one of the active nucleons to a Δ which propagates through the nucleus and then decays to $N+\pi$. Optical distortions of the incident and outgoing nucleons, and the outgoing pion, are taken into account.

In Sec. II we also list and briefly discuss representative amplitudes which contribute to the $(N,N'\pi)$ reactions on a closed-shell nucleus leading to a final state, which is assumed to be a superposition of one-particle–one-hole nuclear excited states. Detailed formulas are collected in Appendixes A–C. The reaction proceeds by exciting one of the active nucleons to a Δ isobar, mediated by virtual meson exchange. In our initial calculations we assume this meson to be a pion. Later in the paper we consider the possible contribution from intermediate ρ mesons. We discuss eight possible amplitudes contributing to this reaction, and show that, for the kinematics chosen, four of these (the pion "preemission" amplitudes) can be negligible. In Sec. III we apply this model to the $^{16}O(p,p'\pi^+)^{16}N^*$ reaction and obtain the differential cross sections for the $0^+\rightarrow 0^-,\ldots,4^-$ transitions. In Sec. III, we also demonstrate the sensitivity of our results to variation of the parameters in our model. In Sec. IV, we summarize our results and suggest experiments on light ($A\leq 40$) targets which can provide relatively stringent tests of the reaction mechanism proposed in this paper.

II. FORMALISM

In this section, we outline the formalism adopted to calculate the exclusive $(N,N'\pi)$ reaction on light nuclei. Calculation of the full amplitude naturally divides into three parts.

(a) We assume a single hard scattering of the projectile nucleon with one of the target nucleons; the pion is produced through the reaction $N+N\rightarrow N+N+\pi$ in the nuclear medium. For the kinematic region investigated in this paper it is assumed that this process is dominated by the formation of an intermediate $\Delta(1232)$ isobar. We discuss the parameters which appear in this scattering and outline a procedure for incorporating intermediate Δ-nucleus interactions into this reaction model.

(b) We include optical distortions of the outgoing pion, and both the incoming and outgoing nucleons, with the residual nucleus. We discuss the parameters of the optical potentials for the hadrons in this model. In addition, to simplify numerical calculations the various distorted waves are expanded in a plane-wave basis, and this approximation is reviewed in detail.

(c) We consider exclusive reactions leading from the ground state of a closed-shell nucleus to one-particle–one-hole states in the final nucleus. We discuss the nuclear structure model and single-particle orbitals utilized for the initial and final many-particle nuclear bound-state systems.

The hard scattering process which produces the pion can be expressed schematically as the sum of several terms. These may be collected into various groups. First, there are two different time-ordered amplitudes for pion production: the "postemission" amplitudes in which the final pion is emitted when the intermediate isobar decays, and the "preemission" amplitudes where the pion is emitted in the initial vertex when the isobar is formed. Antisymmetrizing the continuum and bound nucleons in initial and final states leads to another set of amplitudes.

For example, the four distinct amplitudes, named "postemission," are shown schematically in Fig. 1. We assume that exchange of a virtual meson between two nucleons excites one of them to a Δ isobar, and the outgoing pion is emitted when the isobar decays. Figure 2 shows

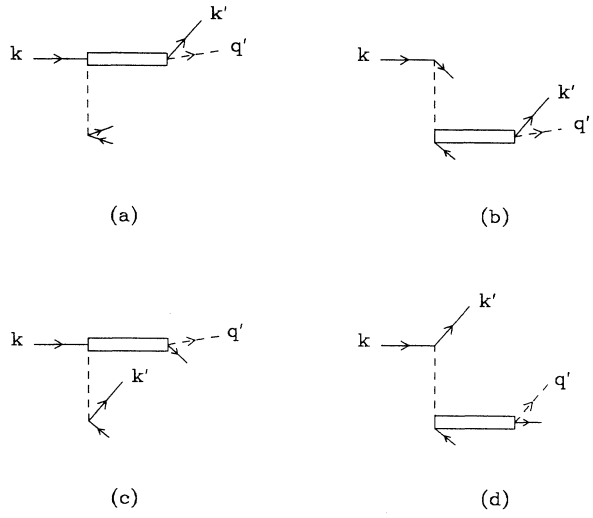

FIG. 1. The postemission diagrams for the $(N,N'\pi)$ reaction. (a)–(d) represent amplitudes A_1, B_1, C_1, and D_1, respectively, from Eq. (2.2). The dashed line represents a pion, solid lines with (without) momentum labels represent continuum (bound) nucleons, and the narrow rectangle represents a $\Delta(1232)$.

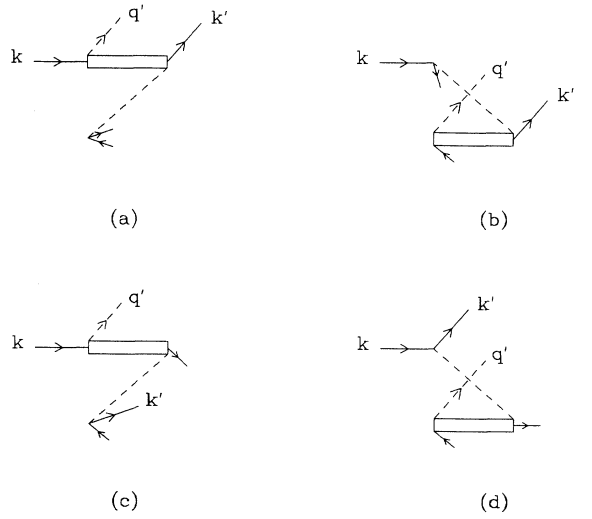

FIG. 2. Same as Fig. 1, except for the preemission amplitudes A_2, B_2, C_2, and D_2.

the four corresponding amplitudes for the "preemission" process, where the outgoing pion is emitted at the initial vertex and the isobar decays to a nucleon plus a virtual meson. For the low energies involved in these calculations, the "preemission" amplitudes of Fig. 2 turn out to be negligible compared to the "postemission" amplitudes in the $(p,p'\pi^+)$ reaction. For the dominant postemission amplitudes (see Fig. 1) the basic picture is that of a projectile nucleon, whose energy is at or above threshold for Δ excitation, interacting with a target nucleon via the exchange of a virtual intermediate meson. This results in the formation of an intermediate Δ which decays into a pion and a nucleon. One of the two final nucleons is detected (along with the pion), while the other nucleon is left in an excited nuclear orbital. In the present simple nuclear model we assume a closed-shell $J=T=0$ initial target and a final nuclear excited state which can be written as a linear combination of pure particle-hole states.

The incident nucleon-nucleus c.m. expression for the exclusive $(N,N'\pi)$ differential cross section for an unpolarized initial nucleon can be written as

$$\frac{d^3\sigma}{d\Omega' d\Omega_\pi dE'}=\frac{10^4}{2(2\pi)^5}\frac{k'k_\pi E'E}{k(1+E/E_A)}|\bar{T}_{fi}|^2\,, \tag{2.1}$$

where k (k') is the initial (final) detected nucleon momentum, E (E') is the initial (final) nucleon energy, k_π is the pion momentum, and E_A is the initial nuclear target energy in the c.m. system. The units for the cross sections in Eq. (2.1) are μb/sr^2 MeV, and we use units where $\hbar=c=1$. The amplitude $\bar{T}_{fi}$ contains effects due to distortions, the reaction mechanism, and the nuclear structure model adopted. A detailed listing of the contributions of the diagrams shown in Figs. 1 and 2 is given in the Appendixes.

To evaluate the scattering amplitude, we consider a reaction leading to a particle-hole state where, for example, the quantum numbers of the final particle state are (l_p,s_p,j_p). We adopt j-j coupling to describe the final nuclear particle-hole state. The selection rules for the various amplitudes are most transparent in L-S coupling. Thus we calculate transition amplitudes using L-S coupling for the final particle-hole state and then transform to the j-j basis using standard recoupling coefficients; this yields the following form for the transition amplitude $\bar{T}_f$:

$$|\bar{T}_{fi}|^2=\frac{1}{2}\sum_{s_{z_i},s_{z_f}}\sum_{J_z}\left|\sum_{L,S}\sum_{j_p,j_h}\sum_{l_p,l_h}\hat{j}_p\hat{j}_h\hat{L}\hat{S}\begin{Bmatrix} l_p & l_h & L\\ s_p & s_h & S\\ j_p & j_h & J\end{Bmatrix}\alpha^{l_p,l_h}_{j_p,j_h,J}\sum_{i=1}^{2}(A_i-B_i-C_i+D_i)\right|^2\,, \tag{2.2}$$

where we use the notation $\hat{L}\equiv\sqrt{2L+1}$. In Eq. (2.2), the terms with $i=1$ correspond to the postemission amplitudes shown in Fig. 1, and those with $i=2$ correspond to the preemission amplitudes of Fig. 2. We use the term "projectile excitation" to describe those amplitudes [e.g., Fig. 1(a)] where the projectile nucleon is excited to an isobar; those [e.g., Fig. 1(d)] where a target nucleon is excited to a Δ are called "target excitation" amplitudes. Finally, those amplitudes where the outgoing continuum nucleon is identical to the projectile are referred to as "direct" amplitudes, and those where the incident nucleon is captured into a bound orbital are called "ex-

change" amplitudes.

The amplitude A_1 of Eq. (2.2) is given schematically by Fig. 1(a); it represents the direct projectile excitation postemission amplitude, since the projectile nucleon is excited to a Δ which decays into a continuum nucleon. The amplitude C_1 is obtained from A_1 by exchanging the two final-state nucleons, and is shown in Fig. 1(c); it is the exchange projectile excitation where the nucleon emitted from Δ decay is captured in a bound nuclear orbital state, and the target nucleon which participated in the hard scattering process is ejected from the nucleus. Figures 1(d) and 1(b) show the direct target excitation and exchange target excitation amplitudes, respectively. Conservation of angular momentum and isospin results in nuclear final-state selection rules for some of the amplitudes. These are discussed more fully in the Appendixes and are briefly summarized later in this section. For illustrative purposes, we undertake a detailed evaluation of a single amplitude, the direct projectile excitation term shown in Fig. 1(a). Calculation of the remaining amplitudes follows rather directly and full equations are presented in the Appendixes.

A. Formalism for evaluating the amplitudes

Evaluation of the amplitude A_1 [Fig. 1(a)] is obtained by combining the expressions for the relevant distorted waves, reaction mechanism, and nuclear structure. Before discussing the amplitude we briefly summarize the procedure used for obtaining these constituent parts.

1. The reaction mechanism

The basic features of the reaction mechanism assumed were discussed by Jain, Londergan, and Walker [14], who carried out a plane-wave calculation of this reaction. We assume an effective nonrelativistic Lagrangian of the form

$$\begin{aligned}\mathcal{L}_{\rm NR}=&\frac{f_{\pi NN}}{m_\pi}\bar{\chi}_N\boldsymbol{\sigma}\cdot\mathbf{q}\boldsymbol{\tau}\chi_N\cdot\boldsymbol{\phi}+\frac{f_{\pi N\Delta}}{m_\pi}\bar{\chi}_\Delta\mathbf{S}\cdot\mathbf{q}\mathbf{T}\chi_N\cdot\boldsymbol{\phi}\\&+\frac{f_{\rho NN}}{m_\rho}\bar{\chi}_N(\boldsymbol{\sigma}\times\mathbf{q})_\lambda\boldsymbol{\tau}\chi_N\cdot(\boldsymbol{\rho}_\lambda)^\dagger\\&+\frac{f_{\rho N\Delta}}{m_\rho}\bar{\chi}_\Delta(\mathbf{S}\times\mathbf{q})_\lambda\mathbf{T}\chi_N\cdot(\boldsymbol{\rho}_\lambda)^\dagger\ ,\end{aligned}\tag{2.3}$$

where $\boldsymbol{\sigma}$ and $\boldsymbol{\tau}$ are the Pauli spin and isospin matrices, $\mathbf{S}$ and $\mathbf{T}$ are 2×4 transition matrices that connect the nucleon and Δ spin and isospin wave functions, q is the meson wave number, $\boldsymbol{\phi}$ is the pion field, $\boldsymbol{\rho}_\lambda$ is the λth spin component of the ρ field (which is a vector in both spin and isospin), and m_π and m_ρ are the π and ρ masses, respectively. For the coupling constants we use $f_{\pi NN}=1.009$, $f_{\pi N\Delta}=2.156$, $f_{\rho NN}=7.811$, $f_{\rho N\Delta}=16.694$ [15,16]. The π-nucleon coupling constants $f_{\pi NN}$ and $f_{\pi N\Delta}$ are multiplied by the form factor $F_\pi(q)$, and the ρ-nucleon coupling constants $f_{\rho NN}$ and $f_{\rho N\Delta}$ are multiplied by $F_\rho(q)$, where we choose form factors of monopole type

$$F_i(q)=\frac{\Lambda^2-m_i^2}{\Lambda^2-\omega^2+\mathbf{q}^2}\ ,\tag{2.4}$$

We use the same cutoff mass $\Lambda=1200$ MeV [16] for both the pion and the ρ meson.

We next assume a propagator for a $\Delta(1232)$ isobar formed in the nucleus and propagating through the nuclear medium. The Δ propagator contains an energy denominator which we parametrize as

$$D_\Delta(q^\Delta,\omega^\Delta)=\omega^\Delta-T_\Delta-M_\Delta-\mathcal{V}_\Delta(q^\Delta,\omega^\Delta)+i\Gamma/2\ .\tag{2.5}$$

In Eq. (2.5), $\mathcal{V}_\Delta(q^\Delta,\omega^\Delta)$ is the real part of the nuclear potential experienced by a Δ with three-momentum $\mathbf{q}^\Delta$ and energy ω^Δ. We approximate this with an effective local potential of depth -35 MeV, appropriate for an incident nucleon energy of ≈400 MeV [8,14]. For the Δ kinetic energy T_Δ, we use the nonrelativistic form

$$T_\Delta=(\mathbf{q}^\Delta)^2/2M_\Delta\ .\tag{2.6}$$

The quantity Γ in Eq. (2.5) represents the width of the isobar in the nucleus. This could be modified from the free isobar width by nuclear interactions and thus includes the imaginary part of the isobar self-energy in the medium, which we parametrize by

$$\Gamma=P\Gamma_0+\Gamma_A\ .\tag{2.7}$$

Here $\Gamma_0=115$ MeV is the free width, P is a Pauli factor that accounts for suppression of the decay $\Delta\rightarrow N+\pi$ due to the Pauli principle, and Γ_A is the absorption width due to the Δ-nucleus collisions. In this preliminary study, we use the free width $\Gamma=\Gamma_0$, because the combined effects of including the Pauli factor and the absorption width tend to cancel somewhat [16,17]. A zero range approximation has been utilized in treating the Δ propagation, which is equivalent to fixing the Δ momentum. This results in no change of form for the postemission direct projectile excitation amplitude (amplitude A_1), in the plane-wave approximation. However, we will test and discuss this approximation when we carry out the full distorted-wave calculation later in Sec. III.

Our model involves a virtual meson exchanged between nucleon and isobar. Initially we take this meson to be a pion; the energy denominator for pion propagation in the nucleus is given by

$$D_\pi(q,\omega)=\omega^2-\mathbf{q}^2-m_\pi^2-\Pi(q,\omega)\ ,\tag{2.8}$$

where $\Pi(q,\omega)$ is the self-energy of a pion with three-momentum $\mathbf{q}$ and energy ω. To estimate this we have calculated the pion self-energy in infinite nuclear matter, assuming an effective Fermi momentum $k_F=210$ MeV/c and a Landau-Migdal parameter $g'=0.7$. Figure 3 shows schematically the contributions to the intermediate pion self-energy arising from the particle-hole, delta-hole, and short-range repulsive terms, respectively. Explicit forms of the self-energy contributions are given in Appendix B of Ref. [14]. In Sec. III we will discuss the dependence of our results on the values chosen for k_F and g'. For completeness we list here the form for the inverse of the ρ propagator

$$D_\rho(q,\omega)=\omega^2-\mathbf{q}^2-m_\rho^2+i\epsilon\ .\tag{2.9}$$

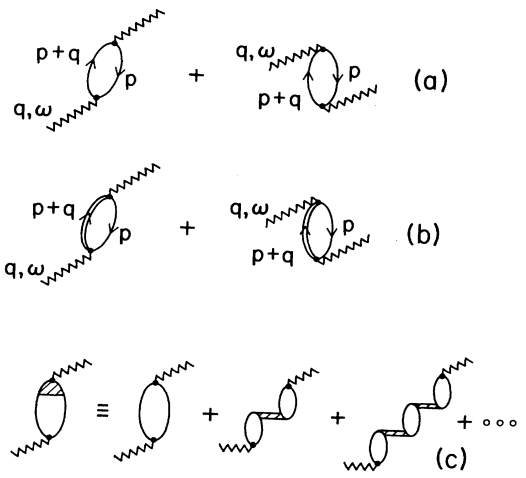

FIG. 3. The contributions to self-energy of the virtual pion. (a) shows the direct and exchange particle-hole contributions. (b) shows the direct and exchange Δ-hole contributions. (c) shows the contribution from the short-range repulsion in the baryon-baryon interaction.

In this preliminary investigation we have not included the nuclear self-energy of the ρ.

2. *Distorted waves*

We have used proton and pion distorted waves obtained from standard optical potentials. The general forms are the same as the ones used in an earlier (p,π) theoretical study [1]. For completeness, we summarize below and in Tables I and II the forms and parameters adopted. The optical potential parameters are obtained from fits to elastic-scattering cross sections at the appropriate incident energies. These potentials are then inserted in the radial Schrödinger (Klein-Gordon) equation for the nucleon (pion) which is then solved to obtain radial distorted waves for each partial wave.

Expressions for the scattering amplitudes are obtained by inserting the resulting nuclear wave functions into integrals containing various potentials and propagators. These integrals are reasonably tedious to calculate but can be done analytically in a plane-wave approximation where the scattering wave functions are just spherical Bessel functions. To expedite the calculation of these integrals (and because the plane-wave integrals have previously been evaluated), we expand the distorted wave functions as a sum of Bessel functions of different momenta, with (complex) coefficients and expansion obtained by a minimization procedure at each partial wave and energy [18]. We obtain a general fit to the expansion coefficients as a function of the asymptotic momentum of the corresponding scattering particle [17]. The explicit expressions for the distorted wave functions are summarized below.

The incoming nucleon distorted wave can be written as

$$\chi_\nu^+(\mathbf{k},\mathbf{r})=4\pi\sum_{l,m}\sum_{j,\nu'}(i)^l C^{l\ 1/2j}_{m\,\nu\ m+\nu}C^{l}_{m+\nu-\nu'\,\nu'\ m+\nu}\times Y_m^{l*}(\hat{\mathbf{k}})Y^l_{m+\nu-\nu'}(\hat{\mathbf{r}})U_{l,j}(k,r)\ , \quad (2.10)$$

where the radial function $U_{l,j}(k,r)$ is the solution to the Schrödinger equation

$$\left[-\frac{1}{2\mu}\frac{d^2}{dr^2}+\frac{l(l+1)}{2\mu r^2}+V\left[l,j=l\pm\frac{1}{2},r\right]-E\right]\times U_{l,j=l\pm1/2}(k,r)=0\ . \quad (2.11)$$

In Eq. (2.11), μ is the nucleon reduced mass, E is the energy, and k the wave number in the nucleon-nucleus c.m. system; these are related by the relativistic expression $E^2=k^2+\mu^2$. The nucleon-nucleus optical potential, $V(l,j,r)$ has the form

$$V(l,j,r)=V_1f_1+iW_2f_2-\frac{2}{r}\left[V_3\frac{df_3}{dr}+iW_4\frac{df_4}{dr}\right](\mathbf{l}\cdot\boldsymbol{\sigma})+V_{\text{Coul}}\ , \quad (2.12)$$

where V_1 (W_2) is the strength of the real (imaginary) central potential with V_3 and W_4 being the corresponding strengths of the spin-orbit potential. The uniform charge distribution Coulomb potential (V_{Coul}) is nonzero for protons only. The f_i's are the Woods-Saxon form factors

$$f_i(r)=\frac{1}{1+\exp[(r-R_i)/a_i]}\ , \quad (2.13)$$

with R_i the potential well radius and a_i the skin thickness. The parameters utilized are listed in Table I, and are taken from Refs. [19,20]. In this paper we consider only spin-averaged cross sections; as the full distorted-wave expressions take a great deal of computer time to evaluate, we average the two spin wave functions for a given angular momentum; hence, we define

$$\psi_l(k,r)=\frac{U_{l,l+1/2}(k,r)+U_{l,l-1/2}(k,r)}{2}\ . \quad (2.14)$$

TABLE I. The nonrelativistic p-^{16}O optical potential parameters at various proton laboratory kinetic energies [19].

T_p (MeV)	V_1	R_1	a_1	W_2	R_2	a_2	V_3	R_3	a_3	W_4	R_4	a_4
135	−10.897	1.494	0.495	−19.897	1.151	0.594	−14.268	0.877	0.433	6.181	1.050	0.402
200	−9.935	1.533	0.539	−20.465	1.153	0.573	−13.893	0.889	0.463	6.104	1.022	0.406
250	−4.00	1.470	0.430	−17.500	1.190	0.590	−12.00	0.930	0.490	8.800	1.020	0.470
318	−9.338	0.651	0.536	−20.982	1.328	0.570	−14.830	0.959	0.523	19.000	0.992	0.575
354	−1.100	1.380	0.350	−18.500	1.240	0.630	−9.200	0.960	0.560	14.400	0.980	0.570
500	−11.796	1.277	0.332	−17.745	1.186	0.682	4.804	0.903	0.556	21.906	1.037	0.637

TABLE II. The π-^{16}O optical potential parameters at various pion laboratory kinetic energies [19,20].

T_π (MeV)	b_0	c_0	B_0	C_0
49.97	(−0.0708, 0.0060)	(0.7131, 0.0275)	(0.1481, −0.0456)	(0.6448, 0.9766)
81.87	(−0.0893, 0.0133)	(0.8058, 0.1125)	(0.3409, −0.2844)	(0.3940, 1.7322)
90.03	(−0.0932, 0.0154)	(0.8236, 0.1490)	(0.3783, −0.3409)	(0.3921, 1.9697)
97.02	(−0.0964, 0.0172)	(0.8344, 0.1867)	(0.4052, −0.3885)	(0.4205, 2.1982)
179.63	(−0.1212, 0.0417)	(0.0846, 0.7228)	(0.0000, 0.0000)	(0.0000, 0.0000)

With this approximation, Eq. (2.10) for the incoming nucleon distorted wave has the form

$$\chi^+(\mathbf{k},\mathbf{r})=4\pi\sum_{l,m}(i)^l Y_m^{l*}(\hat{\mathbf{k}})Y_m^l(\hat{\mathbf{r}})\psi_l(k,r)\ , \tag{2.15}$$

and for the outgoing nucleon distorted wave we have

$$\chi^{-*}(\mathbf{k},\mathbf{r})=4\pi\sum_{l,m}(-i)^l Y_m^{l*}(\hat{\mathbf{k}})Y_m^l(\hat{\mathbf{r}})\psi_l(k,r)\ . \tag{2.16}$$

We now approximate the spin-averaged distorted wave functions by expanding them in a basis of spherical Bessel functions,

$$\psi_l(k,r)=\sum_i a_{l,i}^p(k)j_l(k_i^p r)\ . \tag{2.17}$$

In Eq. (2.17) we used a three-term approximation for the distorted nucleon wave function. The three wave numbers were centered about the asymptotic wave number k with the dispersion in the proton wave number Δk^p chosen to be 1.5 fm^{-1}, i.e.,

$$k_i^p=k-1.5\ ,\ k\ ,\ k+1.5\ \text{fm}^{-1}\ . \tag{2.18}$$

This procedure and the computer program used to calculate the expansion coefficients are based on the work by Robson and Koshel, and Charlton [18]. Having chosen the dispersion of Eq. (2.18), the expansion coefficients $a_{l,i}^p$ of Eq. (2.17) are obtained by minimizing the difference between the plane-wave expansion and the distorted wave, from $r=0$ out to a matching radius $R=15$ fm. This procedure was followed for each partial wave (we used up to 26 partial waves for the scattering nucleon wave functions). The resulting approximation to the distorted wave function is reasonable; we will show comparison between distorted waves and the plane-wave expansion in the following section.

Similarly, the outgoing pion distorted wave can be written as

$$\chi^{-*}(\mathbf{k},\mathbf{r})=4\pi\sum_{l,m}(-i)^l Y_m^{l*}(\hat{\mathbf{k}})Y_m^l(\hat{\mathbf{r}})\xi_l(k,r)\ , \tag{2.19}$$

where the radial wave function $\xi_l(k,r)$ satisfies the Klein-Gordon equation

$$\left[\nabla_r^2+k^2-\frac{l(l+1)}{r^2}-2\bar{\mu}U_{\text{opt}}\right]\xi_l(k,r)=0\ . \tag{2.20}$$

The pion optical potential is taken to be the potential of Stricker *et al.* [21] obtained by fitting pion-nucleus elastic scattering at pion lab energies in the range 50–180 MeV. If we take the proton and neutron matter densities to be the same then the optical potential of Stricker *et al.* takes the form

$$2\bar{\mu}U_{\text{opt}}=-4\pi[p_1 b_0\rho(r)+p_2 B_0\rho^2(r)]+4\pi\nabla\cdot\left[L(r)\left[\frac{c_0}{p_1}\rho(r)+\frac{C_0}{p_2}\rho^2(r)\right]\right]\nabla\ , \tag{2.21}$$

where $\bar{\mu}$ is the reduced mass of the pion in the pion-nucleus center-of-mass system, and $p_1=1+m_\pi/M$ and $p_2=1+m_\pi/2M$ are the kinematical factors arising in the transformation from the pion-nucleon center of mass to the pion-nucleus center of mass (M and m_π are the nucleon and pion masses, respectively). In Eq. (2.21), $L(r)$ has the form

$$L(r)=\left[1+\frac{4\pi\lambda}{3}\left[\frac{c_0}{p_1}\rho(r)+\frac{C_0}{p_2}\rho^2(r)\right]\right]^{-1}\ , \tag{2.22}$$

where λ is the Lorentz-Lorenz-Ericson-Ericson parameter [22] taken to be 1.6. The values of the optical potential parameters for π-^{16}O elastic scattering at various pion energies are listed in Table II and are taken from Refs. [19,20]. The parameters B_0 and C_0 describe pion absorption and b_0, b_1, c_0, and c_1 are related to the pion-nucleon phase shifts.

We expand the pion distorted waves in a spherical Bessel function basis just like the nucleon waves. For the pion waves we chose a four-term basis with momenta distributed about the asymptotic momentum k. We found that a dispersion $\Delta k^\pi=0.3$ fm^{-1} in the pion wave number gave a good fit to the pion distorted waves for the partial waves we considered (up to ten), and for distances out to $R=10$ fm. With this prescription the pion wave function and dispersed pion momenta have the form

$$\xi_l(k,r)=\sum_i a_{l,i}^\pi(k)j_l(k_i^\pi r)\ ,\qquad k_i^\pi=k-0.3\ ,\ k\ ,\ k+0.3\ ,\ k+0.6\ \text{fm}^{-1}\ . \tag{2.23}$$

3. *Nuclear structure*

We used the Tamm-Dancoff approximation [23] to describe the initial and final nuclear states in our model. That is, we assume the initial nucleus is a closed shell and the final nuclear excited states are taken as a linear combination of pure particle-hole states. We chose harmonic-oscillator orbitals, $\phi_{l,l_z}^n(\mathbf{r})$, for the bound

single-nucleon states with $b = 1.77$ fm as used by Donnelly and Walker [23]. The configuration admixture amplitudes for the specific mass 16 calculation discussed in the next section are taken from the same reference.

B. The postemission direct projectile excitation amplitude (A_1)

Using the wave functions and propagators discussed in the previous section, we can calculate the amplitudes ($A_i - D_i$) appearing in Eq. (2.2) by inserting the relevant quantities and using standard angular momentum coupling techniques. As an example, in this section we present the full equations for the postemission direct projectile amplitude A_1 of Fig. 1(a). The remaining amplitudes are given in Appendix A. Amplitude A_1 corresponds to excitation of the projectile nucleon ($\mathbf{k}$) to a Δ isobar through meson exchange with a target nucleon. The isobar then decays into a final continuum nucleon ($\mathbf{k}'$) and pion ($\mathbf{q}'$), while the target, after exchanging an intermediate meson with momentum ($\mathbf{q}$), is excited to a particle-hole nuclear state of angular momentum (J) and isospin (T). The expression for amplitude A_1 has the form

$$A_1 = A_1^I \frac{f_{\pi NN} f_{\pi N\Delta}^2}{m_\pi^3} \sum_{s_{z_p}, s_{z_h}} \sum_{m_p, m_h} \sum_{L_z, S_z} (-1)^{1/2 - s_{z_h} + l_h - m_h} C^{1/2\ 1/2\ S}_{s_{z_p}\ -s_{z_h}\ S_z} C^{l_p\ l_h\ L}_{l_{z_p}\ -m_h\ L_z} C^{L\ S\ J}_{L_z\ S_z\ J_z}$$
$$\times \int \frac{d^3q}{(2\pi)^3} \int d^3r_1 \int d^3r_2 (4\pi)^3 \sum_{l_1, m_1} \sum_{l_2, m_2} \sum_{l_3, m_3} (i)^{l_1 - l_2 - l_3} Y^{l_1}_{m_1}(\hat{\mathbf{k}}) Y^{l_2}_{m_2}(\hat{\mathbf{k}}') Y^{l_3}_{m_3}(\hat{\mathbf{q}}')$$
$$\times Y^{l_1 *}_{m_1}(\hat{\mathbf{r}}_1) Y^{l_2 *}_{m_2}(\hat{\mathbf{r}}_1) \psi_{l_1}(k, r_1) \psi_{l_2}(k', r_1) \frac{\exp[i\mathbf{q}\cdot(\mathbf{r}_1 - \mathbf{r}_2)]}{D_\pi(q, \omega_A) D_\Delta(q_A^\Delta, \omega_A^\Delta)} \Phi^{n *}_{l_p, m_p}(\mathbf{r}_2) \Phi^{n'}_{l_h, m_h}(\mathbf{r}_2)$$
$$\times \langle s_p | \boldsymbol{\sigma}\cdot\mathbf{q} | s_h \rangle \langle s_f | [Y^{l_3 *}_{m_3}(\hat{\mathbf{r}}_1) \xi_{l_3}(q', r_1)] (\mathbf{S}\cdot\overleftarrow{\nabla})(\mathbf{S}^\dagger\cdot\mathbf{q}) | s_i \rangle \ , \tag{2.24}$$

where $\psi_{l_1}(k, r_1)$ is the incident nucleon wave function, $\xi_{l_3}(q', r_1)$ is the outgoing pion wave function, and A_1^I is the corresponding isospin factor

$$A_1^I = \sum_{t_{z_p}, t_{z_h}} (-1)^{1/2 - t_{z_h}} C^{1/2\ 1/2\ T}_{t_{z_p}\ -t_{z_h}\ T_z} \langle t_p | \boldsymbol{\tau}\cdot\hat{\boldsymbol{\phi}}^\dagger | t_h \rangle$$
$$\times \langle t_f | (T)_{-\lambda'} (\hat{\boldsymbol{\phi}}'_{-\lambda'})^\dagger (\mathbf{T}^\dagger\cdot\hat{\boldsymbol{\phi}}) | t_i \rangle \ . \tag{2.25}$$

In Eq. (2.25) $\hat{\boldsymbol{\phi}}$ ($\hat{\boldsymbol{\phi}}'$) is the virtual (outgoing final) pion unit vector field in isospin space and λ' is a spherical index for the detected pion isospin projection. For the $(p, p'\pi^+)$ reaction $A_1^I = \sqrt{2}\delta_{T,1}$.

As described in the previous section, we expand the proton and pion distorted waves in a spherical Bessel function basis [Eqs. (2.17) and (2.23), respectively]. Using the expansion for the gradient operator,

$$[Y^{L}_{M *}(\hat{\mathbf{r}}) j_L(Kr)] \mathbf{S}\cdot\overleftarrow{\nabla}$$
$$= (i)^{L-1} K \sum_{s,\mu} \sum_{\nu} (i)^{-s} \frac{\hat{L}}{\hat{s}} (\mathbf{S})_\nu C^{1\ L\ s}_{000} C^{1\ L\ s}_{\nu M \mu} j_s(Kr) Y^{s *}_\mu(\hat{\mathbf{r}}) \ , \tag{2.26}$$

and utilizing angular momentum recoupling algebra, amplitude A_1 may be written as

$$A_1' = 64\sqrt{2\pi}(-1)^{l_h + j + S'} (i)^{1-L} \hat{l}_p \hat{l}_h \delta_{S,1} \hat{S}' \frac{f_{\pi NN} f_{\pi N\Delta}^2}{m_\pi^3} C^{L\ 1\ J}_{0\ 0\ 0} \frac{A_1^I}{D_\Delta(q_A^\Delta, \omega_A^\Delta)}$$
$$\times \sum_{l_1, \ldots, l_4 L_3, l_8 i, j, \epsilon} \alpha_{l_1, i} \beta_{l_2, j} \gamma_{l_3, \epsilon} q'_\epsilon (i)^{-l_1 + l_2 - L_3 + l_4}$$
$$\times \frac{\hat{l}_1 \hat{l}_2 \hat{l}_3 \hat{L}_3 \hat{l}_4}{\hat{l}_8} C^{1\ l_3\ L_3}_{0\ 0\ 0} C^{1\ J\ l_4}_{0\ 0\ 0} \{[Y^{l_1}(\hat{\mathbf{k}}) \otimes Y^{l_2}(\hat{\mathbf{k}}')]^{l_8} \otimes Y^{l_3}(\hat{\mathbf{q}}')\}^{l_9}_{m_9}$$
$$\times \begin{Bmatrix} \frac{1}{2} & 1 & \frac{3}{2} \\ 1 & \frac{1}{2} & S' \end{Bmatrix} \begin{Bmatrix} l_4 & l_8 & L_3 \\ l_3 & 1 & l_9 \end{Bmatrix} \begin{Bmatrix} 1 & J & l_4 \\ l_9 & 1 & S' \end{Bmatrix}$$
$$\times \int_0^\infty dq \frac{q^4 f(q)}{D\pi(q, \omega_A)} \left[C^{l_p\ l_h\ L}_{0\ 0\ 0} \int_0^\infty r_2^2 dr_2 R^{n *}_{l_p}(r_2) R^{n'}_{l_h}(r_2) j_L(qr_2) \right]$$
$$\times \left[C^{l_1\ l_2\ l_8}_{0\ 0\ 0} C^{L_3\ l_4\ l_8}_{0\ 0\ 0} \int_0^\infty r_1^2 dr_1 j_{l_1}(k_i r_1) j_{l_2}(k'_j r_1) j_{L_3}(q'_\epsilon r_1) j_{l_4}(qr_1) \right] . \tag{2.27}$$

In Eq. (2.27) $\alpha_{l,i}$ and $\beta_{l,j}$ are Bessel function coefficients (corresponding to angular momentum l) for the initial- and final-state proton wave functions, respectively [from Eq. (2.17)], and $\gamma_{l,i}$ are the coefficients for the outgoing pion [from Eq. (2.23)]. The factor A_1' of Eq. (2.27) is related to the factor A_1 of Eq. (2.24) by

$$A_1=(-1)^{1/2-s_{z_f}+J_z}C^{1/2\,1/2\,S'}_{s_{z_i}\,-s_{z_f}\,S_z'}C^{J\,S'\,l_9}_{-J_z\,S_z'\,m_{l_9}}A_1' \ . \tag{2.28}$$

We make this substitution since the Clebsch-Gordan coefficients which appear in Eq. (2.28) are common to every term in Eq. (2.2). We therefore redefine the amplitudes A_1, B_1, C_1, and D_1 according to Eq. (2.28); summing these amplitudes and using orthogonality relations for the Clebsch-Gordan coefficients in Eq. (2.2) allows the replacement

$$\sum_{s_{z_i},s_{z_f}}\sum_{J_z}|A_1-B_1-C_1+D_1|^2 = \sum_S{}'\sum_{l_9,m_9}|A_1'-B_1'-C_1'+D_1'|^2 \ . \tag{2.29}$$

Notice that in Eq. (2.27) selection rules require that amplitude A_1 only excite non-normal parity nuclear states and from an initial closed shell with $J=T=0$ this transition can only excite $S=T=1$ final states. These rules can be easily deduced by requiring conservation of total angular momentum, isospin, and parity in Fig. 1(a). Analogous selection rules also can be derived for other amplitudes. Amplitude B_1 can only excite $T=1$ final states and amplitude D_1 cannot produce a $J=0$ final nuclear state (see Appendix A). The significance of this selectivity will become apparent later when we study the cross sections leading to different final nuclear states.

After expanding the distorted waves in a Bessel function basis we obtain expressions for the final amplitudes [cf. Eq. (2.27) and the equations in Appendix A]. These depend upon integrals involving products of three or four spherical Bessel functions. Analytic expressions for such integrals were derived in Ref. [24]. The expressions corresponding to the remaining diagrams in Fig. 1 for postemission amplitudes B_1', C_1', and D_1' are given in Appendix A.

C. Delta finite-range amplitude

The amplitudes derived thus far assume a zero-range approximation for the isobar. With this approximation, the Δ momentum is fixed and both production and decay of the isobar take place at the same point. Allowing the Δ to propagate with finite range requires evaluation of an additional six-dimensional integral (the Δ momentum and an additional spatial coordinate). In plane-wave approximation, the finite-range and zero-range expressions for amplitude A_1 reduce to the same form (see Appendix B). For distorted incident and outgoing scattering particles, the final expression for amplitude A_1' becomes

$$\begin{aligned}
A_1'=&(-1)^{l_h+S'}(i)^{-1-L}128\left[\frac{2}{\pi}\right]^{1/2}\hat{l}_p\hat{l}_h\delta_{S,1}\hat{S}'\frac{f_{\pi NN}f^2_{\pi N\Delta}}{m_\pi^3}C^{L\,1J}_{0\,0\,0}A^I_1\\
&\times\sum_{l_1,\ldots,l_5}\sum_{L_3,l_8}\sum_{i,j,\epsilon}\alpha_{l_1,i}\beta_{l_2,j}\gamma_{l_3,\epsilon}q'_\epsilon(-1)^{l_8}(i)^{l_1+l_2-L_3+l_4}\hat{l}_1\hat{l}_2\hat{l}_3\hat{L}_3\hat{l}_4\hat{l}_8C^{l_1\,l_3\,L_3}_{0\,0\,0}C^{l_2\,l_4}_{0\,0\,0}\\
&\times\{[Y^{l_1}(\hat{\mathbf{k}})\otimes Y^{l_2}(\hat{\mathbf{k}}')]^{l_8}\otimes Y^{l_3}(\hat{\mathbf{q}}')\}^{l_9}_{m_9}\\
&\times\begin{Bmatrix}\frac{1}{2}&1&\frac{3}{2}\\1&\frac{1}{2}&S'\end{Bmatrix}\begin{Bmatrix}l_4&l_8&L_3\\l_3&1&l_9\end{Bmatrix}\begin{Bmatrix}1&J&l_4\\l_9&1&S'\end{Bmatrix}\begin{Bmatrix}l_4&l_1&l_5\\l_2&L_3&l_8\end{Bmatrix}\\
&\times\int_{|k_j'-q_\epsilon'|}^{k_j'+q_\epsilon'}dq^\Delta\frac{(q^\Delta)^2}{D_\Delta(q^\Delta,\omega_A^\Delta)}\left[C^{l_2\,L_3\,l_5}_{0\,0\,0}\int_0^\infty r_3^2dr_3j_{l_2}(k_j'r_3)j_{L_3}(q'_\epsilon r_3)j_{l_5}(q^\Delta r_3)\right]\\
&\times\int_{|k_i-q^\Delta|}^{k_i+q^\Delta}dq\,\frac{q^4f(q)}{D_\pi(q,\omega_A)}\\
&\times\left[C^{l_p\,l_h\,L}_{0\,0\,0}\int_0^\infty r_2^2dr_2R^{n*}_{l_p}(r_2)R^{n'}_{l_h}(r_2)j_L(qr_2)\right]\\
&\times\left[C^{l_1\,l_4\,l_5}_{0\,0\,0}\int_0^\infty r_1^2dr_1j_{l_1}(k_ir_1)j_{l_4}(qr_1)j_{l_5}(q^\Delta r_1)\right] \ .
\end{aligned}\tag{2.30}$$

D. Preemission amplitudes

Equation (2.27) corresponds to the process where the final pion is emitted following the formation and propagation of the isobar. We have also calculated the contribution of the preemission amplitudes where the final pion is emitted when the isobar is formed. For the energies in our calculations, such amplitudes produce isobars far off shell. We shall show that the contributions from preemission amplitudes are much smaller than the dominant postemission terms and are essentially negligible for the $(p,p'\pi^+)$ reaction. For this reason, we have calculated preemission amplitudes only in the plane-wave approximation; these are listed in Appendix C. They can be compared directly to the plane-wave postemission results which are listed in Appendix B.

E. Intermediate ρ meson amplitude

Thus far we have calculated excitation of a Δ arising from exchange of a virtual pion between the incident nucleon and a target nucleon. We can also include contributions where a virtual ρ meson is exchanged between active nucleons. Using the effective Lagrangian of Eq. (2.3) in plane wave approximation, the ρ meson contribution to amplitude A_1 has the form

$$A_\rho = A_1^I \frac{f_{\pi n\Delta} f_{\rho N\Delta} f_{\rho NN}}{m_\pi m_\rho^2} \times \sum_{s_{z_p}, s_{z_h}} \sum_{m_p, m_h} \sum_{L_z, S_z} \sum_{\lambda} (-1)^{1/2 - s_{z_h} + l_h - m_h + \lambda} \times \int d^3 r_1 \int d^3 r_2 \int \frac{d^3 q}{(2\pi)^3} F_A^\rho(q) \frac{\exp[i(\mathbf{k}'+\mathbf{q}'-\mathbf{k}-\mathbf{q})\cdot\mathbf{r}_1]\exp[i\mathbf{q}\cdot\mathbf{r}_2]}{D_\rho(q,\omega_A) D_\Delta(q_A^\Delta, \omega_A^\Delta)} \times C^{1/2\,1/2\,S}_{s_{z_p}\,-s_{z_h}\,S_z} C^{l_p\,l_h\,L}_{m_p\,-m_h\,L_z} C^{L\,S\,J}_{L_z\,S_z\,J_z} \langle s_p | (\sigma \times \mathbf{q})_{-\lambda} | s_h \rangle \times \langle s_f | (\mathbf{S}\cdot\mathbf{q}')(\mathbf{S}^\dagger \times \mathbf{q})_\lambda | s_i \rangle \Phi^{n*}_{l_p, m_p}(\mathbf{r}_2) \Phi^{n'}_{l_h, m_h}(\mathbf{r}_2) \, . \tag{2.31}$$

This term, after extracting the appropriate phase and Clebsch-Gordan coefficient, should be added to the plane-wave pion contribution given in Eq. (B4). Note that in Eq. (2.31) only the tensor coupling of ρ_{NN} appears since the vector part yields zero. The vanishing of the vector contribution occurs because the vector part of the ρ_{NN} coupling is proportional to $\mathbf{q}$; taking the scalar product of this term with the factor $\mathbf{S}^\dagger \times \mathbf{q}$ from the $\rho_{N\Delta}$ term gives zero. After some angular momentum algebra we can write the ρ exchange amplitude as a product of a particle-hole term A_ρ^a times a spin piece A_ρ^b, e.g.,

$$\tilde{A}_\rho = A_1^I \sum_{L_z, S_z} C^{L\,S\,J}_{L_z\,S_z\,J_z} A_\rho^a(L_z) A_\rho^b(S_z) \, . \tag{2.32}$$

Since the ρ meson, like the pion, is an isovector, the isospin factor A_1^I is the same as for the pion, e.g., Eq. (2.25). In Eq. (2.32) the particle-hole and spin factors are defined through

$$A_\rho^a(L_z) = \sqrt{4\pi}(i)^L (-1)^{l_h} \frac{\hat{l}_p \hat{l}_h}{\hat{L}} C^{l_p\,l_h\,L}_{0\,0\,0} Y^{L*}_{L_z}(\hat{\mathbf{q}}_A) A^{n,n'}_{l_p,l_h,L}(q_A) \, , \tag{2.33}$$

$$A_\rho^b(S_z) = -32\pi\sqrt{2} q' q_A^2 (-1)^{S'} \hat{S}' \sum_{\mathcal{L},\mathcal{L}'} \sum_{M'} (-1)^{M'} \hat{\mathcal{L}}' C^{1\,1\,\mathcal{L}}_{0\,0\,0} C^{S'\,\mathcal{L}'\,1}_{-S_z'\,M'\,-S_z} [Y^1(\hat{\mathbf{q}}') \otimes Y^{\mathcal{L}}(\hat{\mathbf{q}}_A)]^{\mathcal{L}'}_{M'} \begin{Bmatrix} \frac{1}{2} & 1 & \frac{3}{2} \\ 1 & \frac{1}{2} & S' \end{Bmatrix} \times \begin{Bmatrix} 1 & 1 & 1 \\ 1 & 1 & \mathcal{L} \end{Bmatrix} \begin{Bmatrix} S' & 1 & 1 \\ \mathcal{L} & 1 & \mathcal{L}' \end{Bmatrix} \delta_{S,1} \, . \tag{2.34}$$

In Eq. (2.33), the particle-hole matrix element $A^{n,n'}_{l_p,l_h,L}$ is defined as

$$A^{n,n'}_{l_p,l_h,L}(q_A) \equiv \int_0^\infty r_2^2 dr_2 R^n_{l_p}(r_2) R^{n'}_{l_h}(r_2) j_L(q_A r_2) \, . \tag{2.35}$$

III. RESULTS AND DISCUSSION

In this section, we use the $(N,N'\pi)$ amplitudes derived in the preceding section to make theoretical predictions for the exclusive ^{16}O$(p,p'\pi^+)^{16}$N* reaction. All results are presented in the overall center of momentum frame. With at least three particles or clusters in the final state, several energies and angles can be varied independently. In this investigatory paper we examine certain sectors of this parameter space. Here we limit our discussion to cases where the incident proton, outgoing proton, and outgoing pion are in the same plane. The outgoing proton and pion scatter on different sides of the beam, looking down on the scattering plane. In the results presented here the scattering angle of the outgoing proton is fixed at $\theta_{p'} = 10°$.

Figure 4 shows the dependence of the momentum transfer to the nucleus, $q \equiv |\mathbf{k}'+\mathbf{q}'-\mathbf{k}|$, with variation of the kinematic variables of the detected particles. Figure 4(a) gives the dependence of the momentum transfer q on the outgoing proton energy for incident proton energies 450 and 800 MeV, when the c.m. pion angle is fixed at $\theta_\pi = 10°$. For an incident proton energy of 450 MeV (a kinematic region dominated by Δ formation), fixing the outgoing proton kinetic energy at 250 MeV gives the momentum transfer to the nucleus its minimum value of approximately 1 fm^{-1}; at this proton incident energy the momentum transfer is close to this value, and relatively

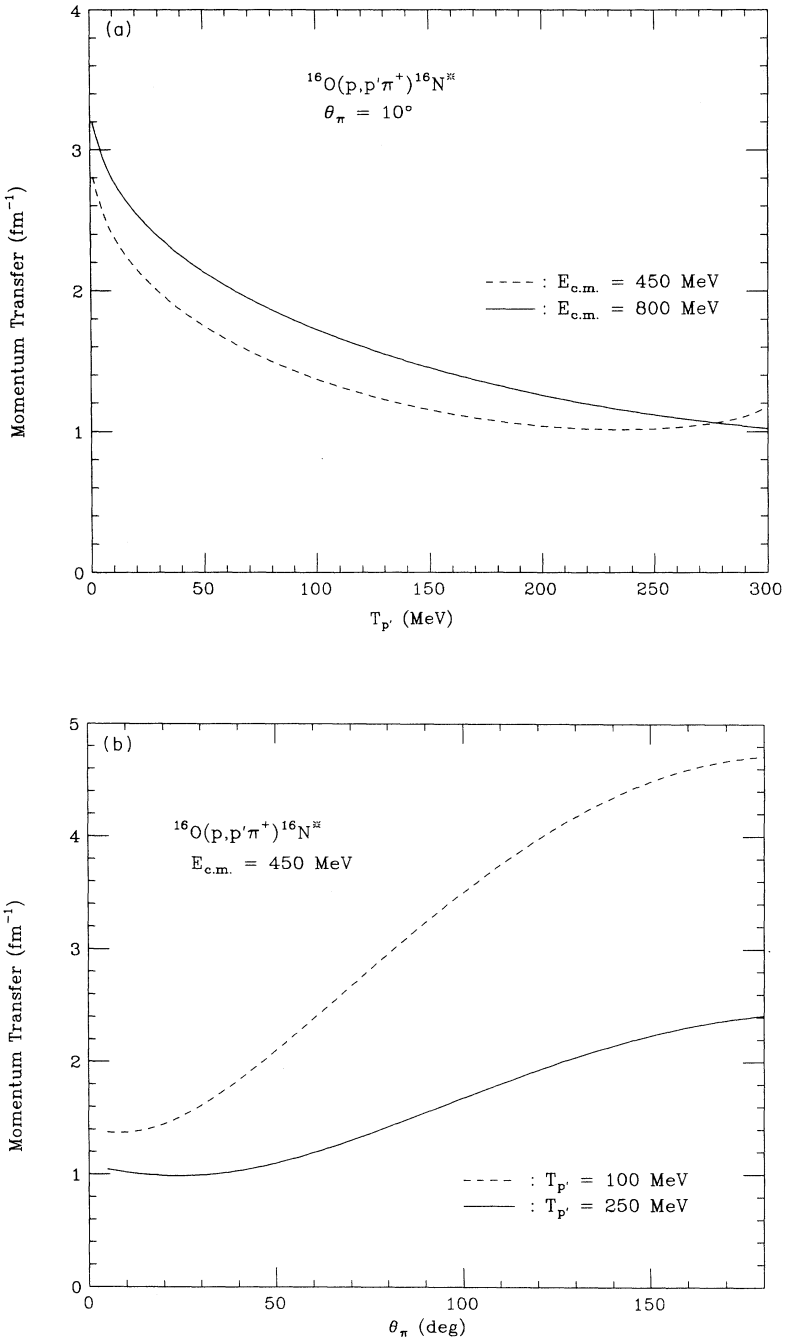

Fig. 4. (a) Momentum transfer to the nucleus for the $(p,p'\pi^+)$ reaction on ^{16}O, as a function of the outgoing proton energy in the overall center of mass frame for c.m. energies of 450 MeV (dashed curve) and 800 MeV (solid curve). (b) Momentum transfer to the nucleus as a function of the outgoing pion angle, for c.m. energy 450 MeV, and for outgoing proton energies of 100 MeV (dashed curve) and 250 MeV (solid curve).

constant, for a wide range of outgoing proton energies between 100 and 300 MeV. Figure 4(b) shows the variation of the momentum transfer with outgoing pion angle, for incident proton energy 450 MeV and outgoing proton energies of 100 and 250 MeV. The nuclear momentum transfer varies approximately linearly with the outgoing pion angle. With these kinematics the nuclear momentum transfer can change considerably as the pion angle is varied: For a 100 MeV outgoing proton, the momentum transfer varies from roughly 1 to 5 fm^{-1} as the pion angle is increased.

In Fig. 5 we evaluate the amplitudes of Eq. (2.2) to predict cross sections for the $^{16}O(p,p'\pi^+)^{16}N^*$ reaction. We assume that ^{16}O is a closed shell and calculate transitions leading to one-particle–one-hole states in ^{16}N. In this figure and other calculations of cross sections, unless stated otherwise, we have calculated only the postemission amplitudes: we will show later that the preemission amplitudes are generally negligible in comparison. We also set the isobar width to its free value, and include only

those amplitudes with an intermediate π meson exchanged between active nucleons (amplitudes involving an intermediate ρ meson will be included later). In Fig. 5 we also neglect the self-energy $\Pi(q,\omega)$ of the exchanged pion.

The most important kinematic variable turns out to be the momentum transfer **q** to the nucleus. Figures 5(a)–5(c) show our results at different values of **q**. The energies and angles of Fig. 5(a) correspond to nuclear momentum transfer $q = 1.05$ fm^{-1} (corresponding to an outgoing pion angle of 5°). At this momentum transfer the 1^- state at approximately 13 MeV excitation energy dominates the spectrum. This is understandable since angular momentum matching conditions generally ensure that low spin transitions are excited more strongly at lower momentum transfer than are high spin transitions.

As we have previously mentioned, the reaction amplitudes shown in Fig. 1 have different angular momentum selection rules; therefore, we expect the relative contributions of the amplitudes A'_1, B'_1, and D'_1 of Eq. (2.29) to vary greatly; indeed, for transitions to some states we expect some amplitudes to vanish. The rectangles in Fig. 5

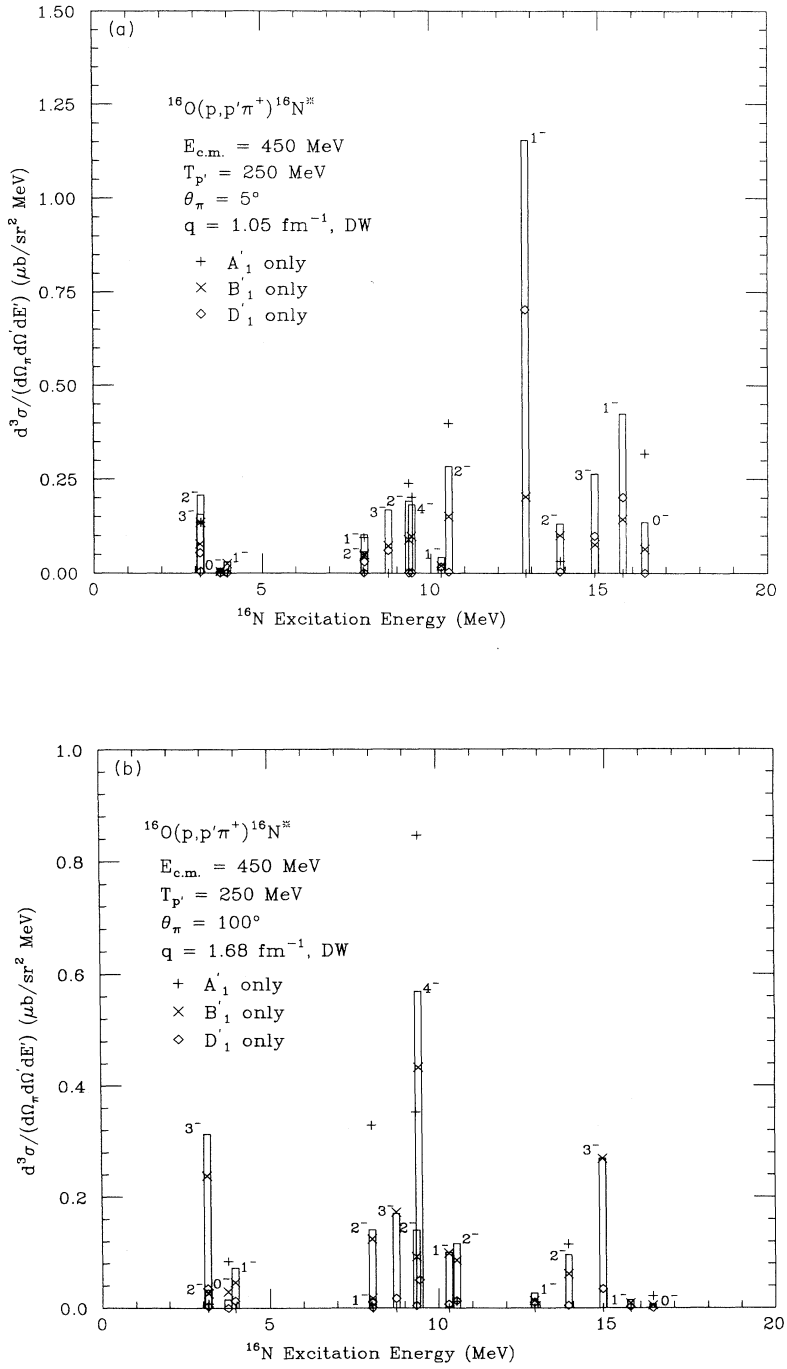

FIG. 5. Excitation energy spectrum for the ^{16}O$(p,p'\pi^+)^{16}$N* reaction leading to one-particle–one-hole final states, for c.m. energy 450 MeV and outgoing proton energy 250 MeV. Rectangle: full calculation with all amplitudes; +: contribution from amplitude A'_1 only; ×: amplitude B'_1 only; ◇: amplitude D'_1 only. (a) outgoing pion angle of 5°, which corresponds to nuclear momentum transfer $q = 1.05$ fm^{-1}; (b) pion angle 100°, corresponding to $q = 1.68$ fm^{-1}; (c) pion angle 130°, corresponding to $q = 2.04$ fm^{-1}.

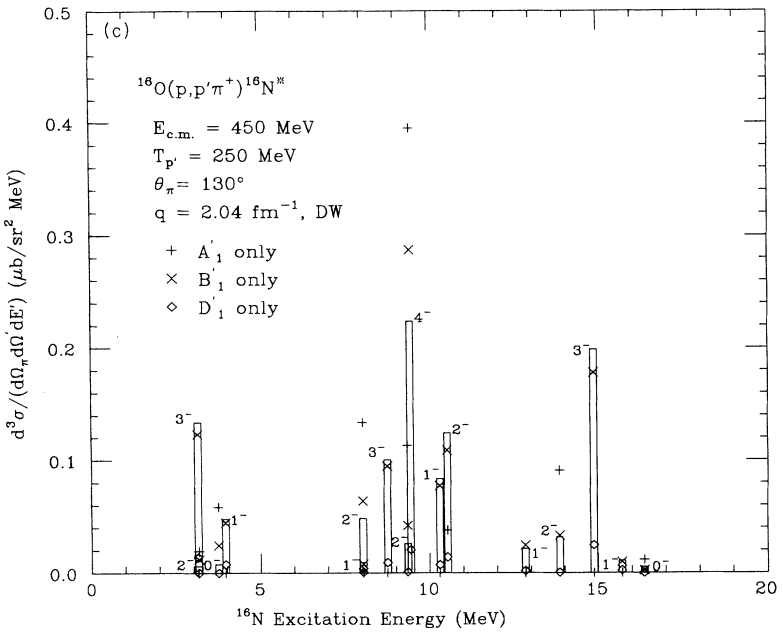

FIG. 5. (*Continued*).

show the full predicted cross sections; + denotes results using amplitude A'_1 only; × shows results using only amplitude B'_1; and ◇ refers to amplitude D'_1 only (amplitude C'_1 is relatively small for any value of L, S, and J). For many of the states, a single amplitude tends to dominate the transition; for some transitions, a single amplitude can produce cross sections which are considerably larger than the full result (due to destructive interference between the dominant amplitude and the others). For example, in Fig. 5(a) the transition to the 1^- state at 13 MeV is dominated by amplitude D'_1, with no contribution from amplitude A'_1 since this is a normal parity transition.

Figure 5(b) shows the same calculated cross sections at nuclear momentum transfer $q=1.68$ fm^{-1}. At this higher momentum transfer the higher angular momentum states have larger cross sections, and indeed the highest available angular momentum state, the 4^- transition at about 9 MeV excitation, dominates the predicted cross sections. For the 4^- transition the amplitude A'_1 is predicted to interfere destructively with the other amplitudes. The amplitude B'_1 dominates the 3^- excitation at 15 MeV. This $0^+ \rightarrow 3^-$ transition exhibits an interesting selectivity in that it is completely dominated by amplitude B'_1. Provided this transition is strong enough to be isolated experimentally, the selectivity of the reaction process could be used to study this individual amplitude.

In Fig. 5(c) we show the same cross sections at momentum transfer $q=2.04$ fm^{-1}. The general trend observed in Figs. 5(a) and 5(b) is continued here. The overall magnitude of the cross sections tends to decrease with increasing momentum transfer. However, some cross sections vary more rapidly than others; for example, comparing Fig. 5(b) and 5(c) we note that as q increases the 4^- state at 9 MeV loses strength compared to the relatively constant strength of the 15 MeV 3^- excitation.

In Fig. 6 we repeat the calculations which were carried out for Fig. 5; however, in Fig. 6 we have included the self-energy of the intermediate pion exchanged between the active nucleons; these self-energy amplitudes are shown schematically in Fig. 3. Comparison of Figs. 5 and 6 shows that inclusion of the pion self-energy increases the predicted cross sections somewhat; however, the self-energy contributions to the amplitude A'_1 are much larger than to the other amplitudes. This is because the energy and momentum carried by the intermediate meson are quite different for the amplitudes of Fig. 1. For transitions to relatively low lying states in the final nucleus, the intermediate pion in amplitude A'_1 has reasonably large momentum but quite small energy. This corresponds to the so-called "acoustic mode" for the pion [16,22,25]. In our model, the pion self-energy is predicted to be quite large for these kinematics. The other amplitudes correspond to different kinematic regions for the virtual pion and we predict relatively small medium enhancement for these terms. From Fig. 6(a) we see that at the relatively low momentum transfer $q=1.05$ fm^{-1}, the 13 MeV 1^- state (which is a normal parity state with no contribution from amplitude A'_1) still dominates the spectrum. Moving to higher momentum transfer we see from Fig. 6(b) that the strength of the 4^- state, which is dominated by amplitude A'_1, is enhanced by a factor of ≈ 5 when we include the pion self-energy. In Fig. 6(c) at $q=2.04$ fm^{-1}, the 4^- state still dominates the spectrum.

In our calculations the pion self-energy contribution to certain amplitudes is significantly enhanced. For example, two of the largest calculated cross sections are to the 4^- state at 9 MeV and the 3^- state at 15 MeV excitation.

For momentum transfer $q = 1.68$ fm^{-1}, the ratio of these states is roughly 1.5 without the pion self-energy [Fig. 5(b)], but a factor of 5 when the self-energy is included [viz. Fig. 6(b)]. Similar comparisons at $q = 2.04$ fm^{-1} predict the ratio of the 4^- transition to the 3^- transition will be 1.1 without self-energy, but 3 when self-energy effects are included.

Inclusion of the pion self-energy enhances different transitions in varying degrees, depending on whether selection rules allow amplitude A to contribute. The degree of expected enhancement clearly depends on the model chosen for the medium effects on the virtual meson. Our calculation assumed a Fermi gas for the nuclear medium. Previous calculations of medium effects on propagating pions [16,26–28] demonstrated that infinite-medium models for meson propagation (such as a Fermi gas) can sometimes significantly overestimate medium effects, relative to more realistic nuclear models like a large-basis random phase approximation (RPA) calculation. Because we predict a marked medium enhancement of transitions with large contributions from amplitude A and only small enhancement from other amplitudes, and since the selection rules pick out different amplitudes in various transitions, then measurement of the relative strengths of transitions to different final states can be used to isolate and study the size of medium

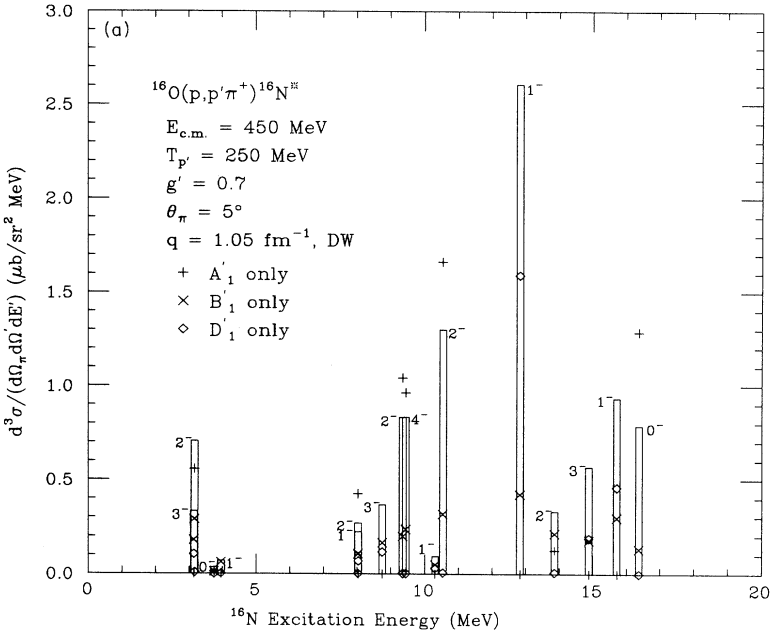

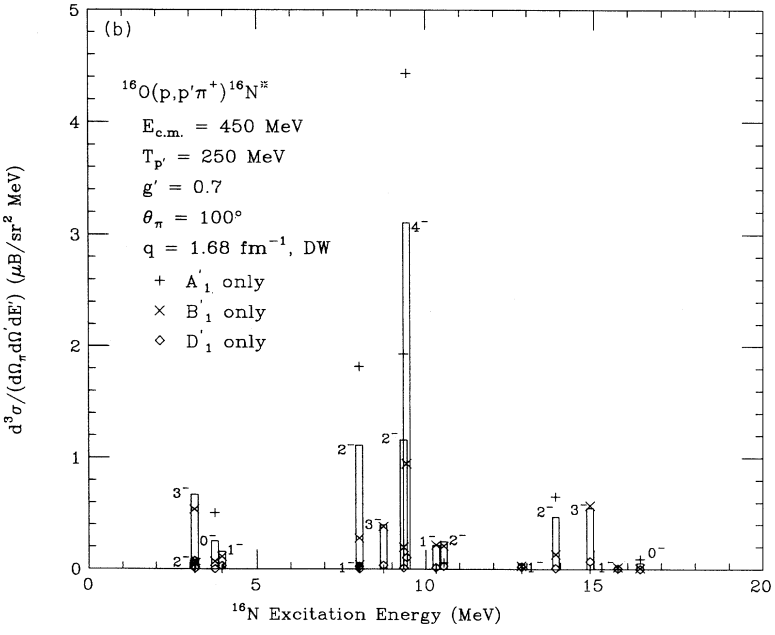

FIG. 6. Same as Fig. 5 but with intermediate pion self-energy contribution included with Landau parameter $g' = 0.7$.

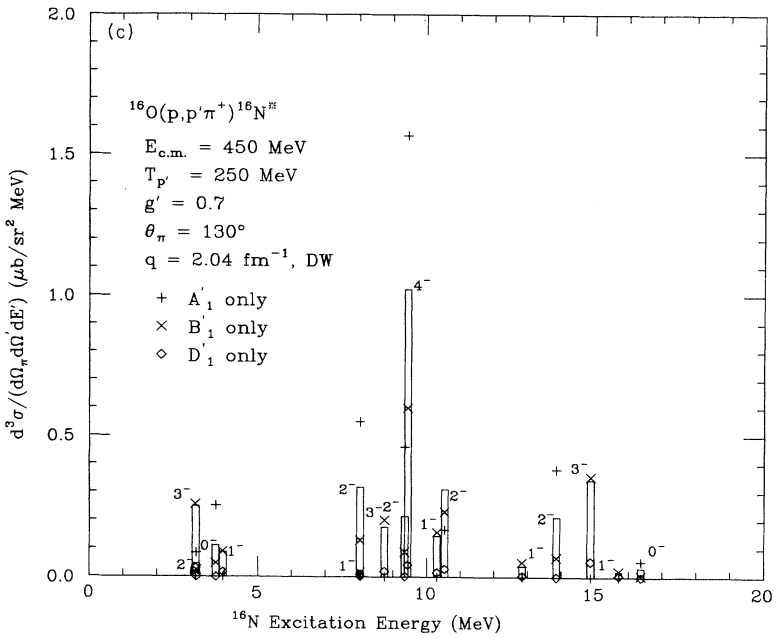

FIG. 6. (*Continued*).

effects.

For example, for $q = 1.68$ fm^{-1}, the ratio of two of the largest cross sections (the 4^- state at 9 MeV and the 3^- state at 15 MeV) is roughly 1.5 (5) without (with) inclusion of the pion self-energy [see Figs. 5(b) and 6(b)]. The ratio is 1.1 (3) without (with) the self-energy for $q = 2.04$ fm^{-1} [see Figs. 5(c) and 6(c)]. Although there are many uncertainties in our theoretical calculations, the ratios of transitions to different final states are relatively insensitive to other variables (such as distortions and nuclear structure), provided these ratios are measured at fixed momentum transfer q. Experimental studies of such transitions may be particularly useful in testing predictions for medium effects in isobar production reactions. Such studies will be the subject of a future report (see Sec. IV).

In Fig. 7 we examine the predicted cross sections to some of the dominant states in the pion production reaction. We assume a proton incident energy of 450 MeV, fix the energy of the outgoing proton at 250 MeV, and plot cross sections versus the c.m. angle of the outgoing pion. In Fig. 7(a) we plot cross sections to the 4^- state at 9 MeV, and in Fig. 7(b) we give cross sections leading to the 1^- state at 13 MeV. The dashed curves give plane-wave calculations with no pion self-energy; dotted curves show plane-wave results when the pion self-energy effects are included; dot-dashed curves show distorted-wave calculations with no pion self-energy effects, and the solid curve shows results when both hadron-nucleus distortions and pion self-energy effects are included.

In Fig. 7(a) we compare these results for the stretched 4^- state. For all four cases the cross section peaks at $\theta_\pi \approx 100°$, corresponding to a nuclear momentum transfer $q \approx 1.7$ fm^{-1}. Inclusion of distortions decreases the plane-wave cross sections by about a factor of 3. Inclusion of the pion self-energy increases the plane-wave cross sections by a factor of 4, and the distorted-wave calculation by a factor of 5. The shape of the predicted cross sections is relatively constant; including distortions tends to decrease the cross sections and adding in the pion self-energy increases the cross sections by roughly the same amount. Thus at this energy and for this final state, the distortions and self-energy corrections tend to cancel, giving a final result within about 30% of the original plane-wave calculation.

Figure 7(b) shows the cross sections for the transition to the 1^- state at 13 MeV. The calculated cross sections have a peak at small pion angle $\theta_\pi \approx 30°$, corresponding to momentum transfer $q = 1$ fm^{-1}. The cross section also shows a dip in the cross section at $\theta_\pi \approx 100°$, which originates from a node in the transition density integral $A^{1,1}_{2,1,1}(q_A)$, in the plane-wave approximation [see Eqs. (2.35) and (B9)]. For the distorted-wave calculation this node has not been completely filled in, although its location has been slightly shifted. For the 1^- state in this kinematic region, inclusion of distortions decreases the plane-wave cross sections by a factor of ≈ 2 for the peak cross sections. Inclusion of self-energy effects increases the cross sections by a factor of 2. Once again, for transitions to the 1^- state the competing effects of nuclear distortions and pion self-energy effects tend to cancel. The extent of this cancellation is highly dependent on kinematic conditions and the particular final state. However, for all of our calculations we find that inclusion of distortions decreases calculated cross sections and self-energy effects tend to increase them. The shape of the predicted cross sections does not differ significantly from plane-wave calculations (except for zeros in plane-wave calculations, which get filled in when distortions are included).

In Fig. 8 we compare the magnitude of the preemission amplitudes of Fig. 2 with the postemission amplitudes. We show this comparison only for the single amplitude $\tilde{D}$ of Figs. 1(d) and 2(d); however, the other amplitudes yield similar results [17]. In Fig. 8 we show plane-wave cross

sections for transitions to a final $(1d)(1p)^{-1}$, $L=1$, $S=1$, $J=2$ state. The dashed curve of Fig. 8 includes only the postemission amplitude $\tilde{D}_1$ shown schematically in Fig. 1(d); the dotted curve shows the cross section from the preemission amplitude of Fig. 2(d); the solid curve shows the full result with both preemission and postemission contributions. The preemission contribution is about one order of magnitude smaller than the dominant postemission term. This occurs because the Δ propagator is farther off shell for the preemission amplitudes; this amplitude also has a smaller isospin factor for the $(p,p'\pi^+)$ cross section compared with the postemission amplitudes (see Appendix C). Hence, the preemission amplitudes are relatively unimportant for the $(p,p'\pi^+)$ reaction (they are never much larger than 10% of the total cross sections) and we therefore neglect them in subsequent calculations.

In Fig. 9 we show the effect of including the exchange of an intermediate ρ meson between the two active nucleons. To give some idea of the importance of this term we have calculated plane-wave cross sections leading to a

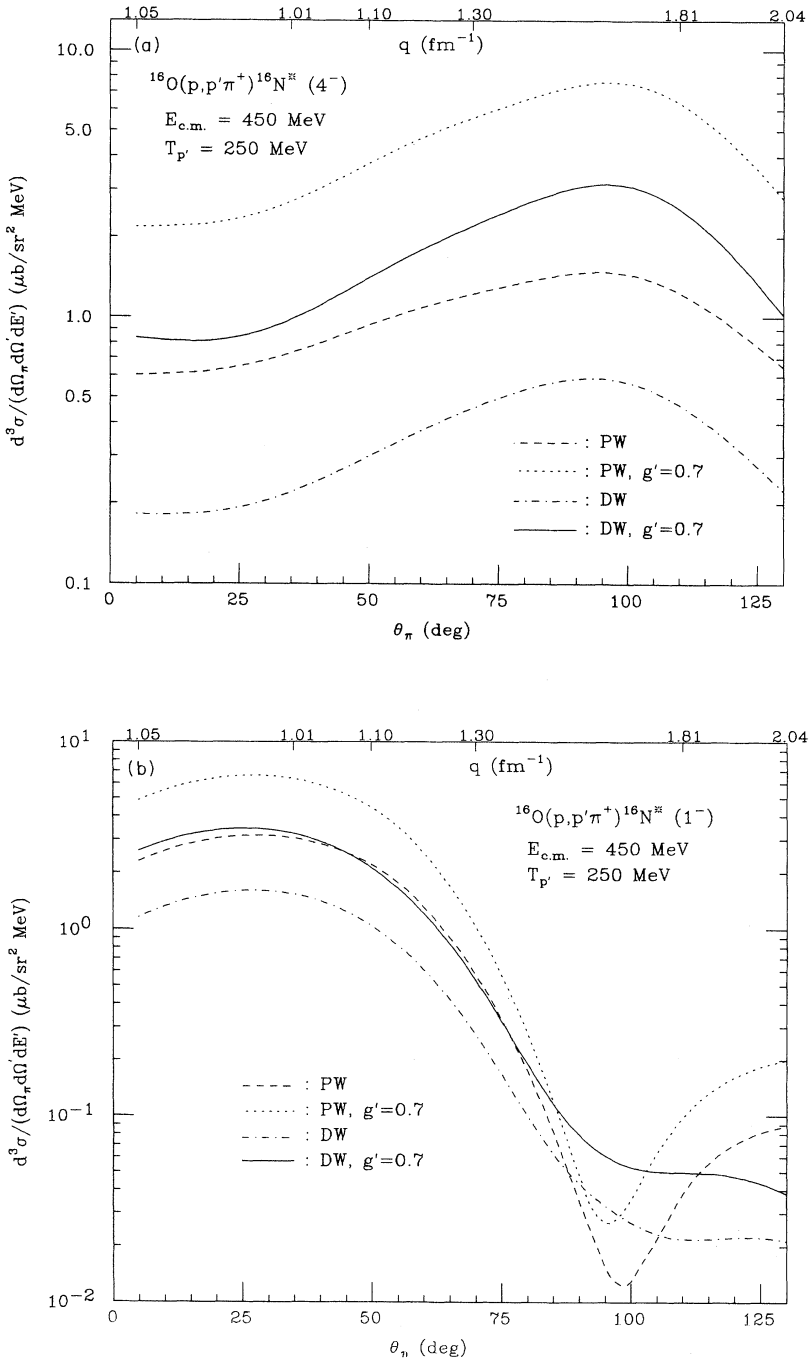

FIG. 7. Differential cross section for the ^{16}O$(p,p'\pi^+)^{16}$N* reaction as a function of outgoing pion angle. Dashed curve: plane-wave calculation; dotted curve: plane-wave calculation including pion self-energy (with $g'=0.7$); dash-dotted curve: distorted-wave calculation without self-energy; solid curve: distorted-wave calculation including self-energy (with $g'=0.7$). (a) Cross section for the $0^+\rightarrow 4^-$ transition; (b) cross section for the $0^+\rightarrow 1^-$ transition.

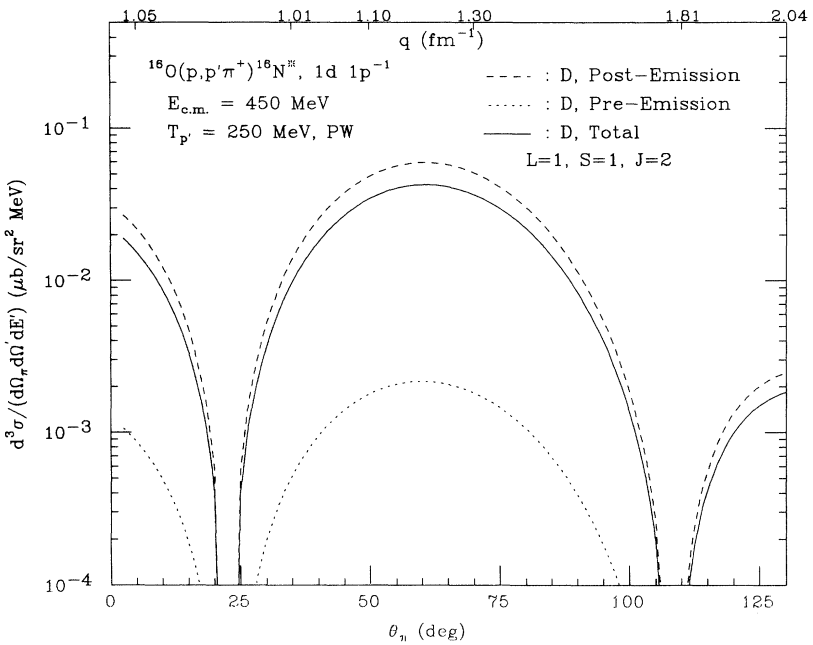

FIG. 8. The differential cross section for the $^{16}O(p,p'\pi^+)^{16}N^*$ reaction as a function of outgoing pion angle for transitions to a $(1d)(1p)^{-1}$, $L=1$, $S=1$, $J=2$ final nuclear state. Calculations have been carried out in plane-wave approximation including only amplitude $\tilde{D}$. Dashed curve: only postemission amplitudes included; dotted curve: only preemission amplitudes; solid curve: both post- and preemission amplitudes included.

final nuclear $(1d)(1p)^{-1}$ state with $L=3$, $S=1$, and $J=4$, including only the amplitude $\tilde{A}_1$. The solid curve shows the cross section including only intermediate pion exchange, the dashed curve shows the result including only the ρ meson contribution, and the dotted curve shows the result including exchange of both mesons. For momentum transfers $q<1.1$ fm^{-1}, the ρ meson makes a negligible contribution to the cross sections. For $q>1.3$ fm^{-1}, the ρ meson contribution is comparable to the pion amplitude; in fact, inclusion of ρ meson exchange increases the peak cross section by a factor of 2. Thus the contribution from the ρ meson can be neglected only for the smallest momentum transfers, and this contribution should be included in subsequent calculations of this process. Some angular momentum selection rules can be derived for ρ exchange; for example, in amplitude $\tilde{A}_1$ an intermediate ρ meson cannot contribute to transitions to a final $J=0$ state.

The dependence of the cross sections on the range Λ of the hadronic form factor [see Eq. (2.4)] is shown in Fig. 10. This figure shows cross sections leading to a final $(1d)(1p)^{-1}$, $L=3$, $S=1$, $J=2$ nuclear state, using distorted waves including only the amplitude A'_1. The solid curve shows results for $\Lambda=1.2$ GeV, the value used

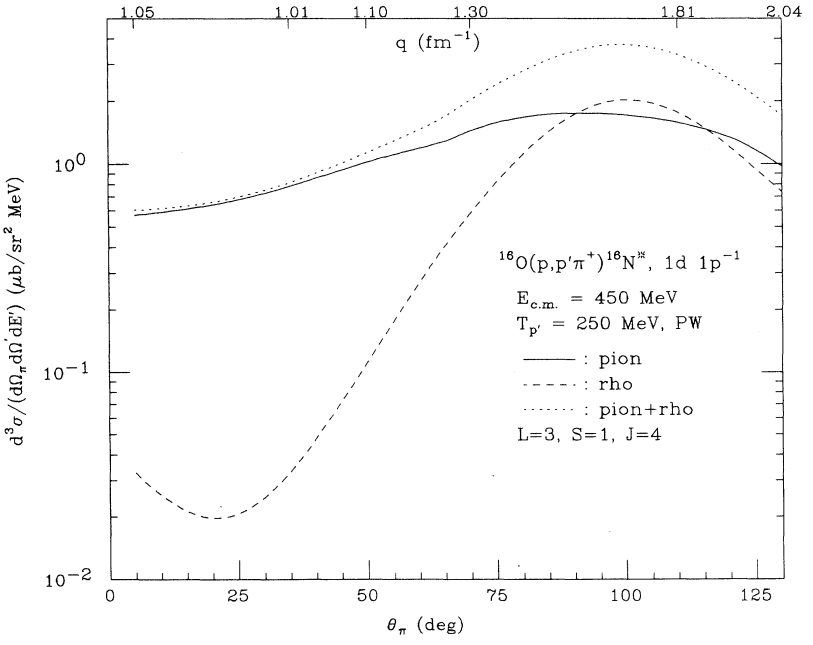

FIG. 9. Differential cross section as a function of outgoing pion angle for transitions to a $(1d)(1p)^{-1}$, $L=3$, $S=1$, $J=4$ final nuclear state in plane-wave approximation, including only amplitude $\tilde{A}_1$. Solid curve: only intermediate pion included; dashed curve: only intermediate ρ meson included; dotted curve: both ρ and π mesons are included in intermediate state.

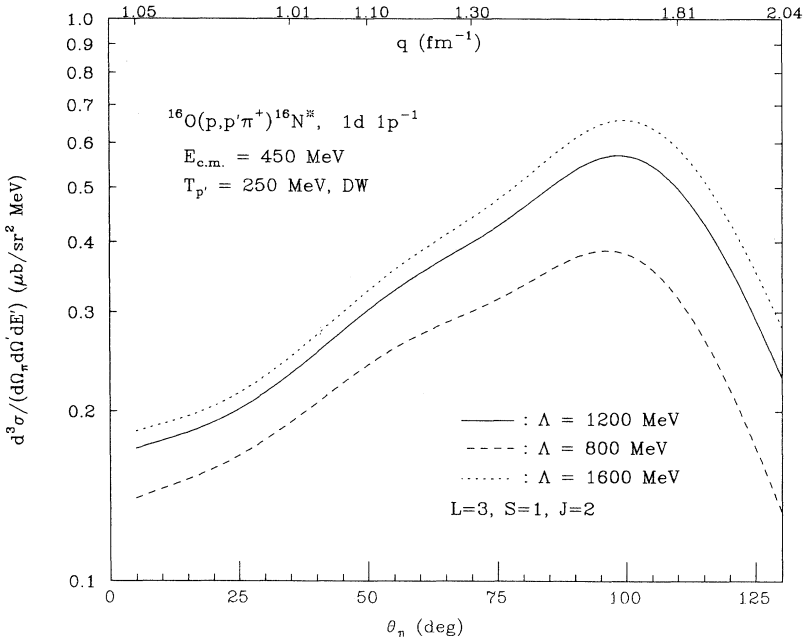

FIG. 10. Dependence of reaction cross sections on range of hadronic form factor. Distorted-wave differential cross section vs outgoing pion angle, including only amplitude A'_1. Solid curve: range $\Lambda=1200$ MeV; dashed curve: $\Lambda=800$ MeV; dotted curve: $\Lambda=1600$ MeV.

throughout this paper; the dotted curve is the result for the harder form factor $\Lambda=1.6$ GeV, and the dashed curve results from the softer form factor $\Lambda=0.8$ GeV. Increasing the form factor from 1.2 to 1.6 GeV increases the calculated cross sections by about 10% without changing their shape; however, reducing Λ to 800 MeV decreases the calculated cross sections by about 40%. In this figure we overestimate the sensitivity of the calculated cross sections to the range of the hadronic form factor; we have changed the form factor range without making compensating changes in the strength of the bare coupling constant, which would be necessary to keep the strength of the $NN\rightarrow NN\pi$ reaction constant.

Next we investigate the dependence of our results on the nuclear interactions of the intermediate pion and isobar. In order to simplify the numerical calculations we examine transitions only to a single nuclear final state, and have included only the largest single amplitude which contributes to this state. We have chosen the transition leading to a $(1d)(1p)^{-1}$, $L=1$, $S=1$, $J=0$ nuclear final state, including only amplitude A'_1.

Our estimate of the self-energy of the intermediate pion was made by assuming the nucleus could be approximated by a Fermi gas with effective Fermi momentum k_F, to which we assigned the value $k_F=210$ MeV/c (this approximation is discussed in Ref. [14]). The short-range repulsion in the baryon-baryon interactions which enter into the pion self-energy were accounted for with a Landau-Migdal term, $g'=0.7$. In Fig. 11 we investigate the dependence of our reaction cross sections on the parameters chosen for the pion self-energy. Figure 11(a) shows the dependence on the parameter k_F. Reducing (increasing) the magnitude of k_F by 100 MeV/c results in a decrease (increase) in the cross section by about a factor of 2. Figure 11(b) shows the effect of varying the Landau parameter g' (we assumed $g'_{N\Delta}=g'_{NN}\equiv g'$). As expected, the cross section increases substantially (by a factor of about 4) when g' is reduced to 0.3, since for values $g'<0.4$ an unphysical pion condensate appears [15,16]. Only the amplitude A_1 is sensitive to changes in g'; the other amplitudes are less sensitive to inclusion of the pion self-energy. The cross section is not appreciably changed when g' is increased.

In order to simplify numerical calculations we assumed a zero-range approximation for the intermediate isobar. Figure 12 shows the effect of including finite-range Δ propagation for amplitude A'_1. There is essentially no difference between the zero- and finite-range calculations for the isobar, except near the deep minimum at $\theta_\pi\approx 100°$. This suggests that the zero-range approximation for Δ propagation gives reliable predictions for this reaction.

Our earlier results assumed that nuclear interactions of the intermediate isobar could be incorporated by a downward shift of the Δ from its free position; this downward shift is chosen to be -35 MeV, in agreement with isobar-hole calculations in this energy region [8]. Figure 13(a) shows the sensitivity of the cross section to the Δ-nucleus potential, $\mathcal{V}_\Delta$: the solid curve shows results when $\mathcal{V}_\Delta=-35$ MeV, the dashed curve $\mathcal{V}_\Delta=-70$ MeV, and the dotted curve gives results when $\mathcal{V}_\Delta=0$. As $\mathcal{V}_\Delta$ becomes more attractive the cross section is enhanced for $\theta_\pi<100°$.

One expects two competing nuclear effects on the width of the isobar. The intermediate decay $\Delta\rightarrow N+\pi$ will be suppressed in medium, due to Pauli principle effects which require the nucleon in this decay to be antisymmetrized with those in the nucleus. We have approximated this by the Pauli factor P in Eq. (2.7). Previously we have set $P=1$, which corresponds to ignoring Pauli effects. Figure 13(b) shows the effects of varying the Pauli factor, P. The solid curve corresponds to $P=1$

and the dashed curve to $P=0.7$. The resulting cross sections are quite similar, and cross sections differences of more than 10% occur only where the overall cross section is very small; this effect decreases the width of the isobar in the nucleus and hence tends to increase the calculated cross sections.

While the Pauli effects tend to decrease the width of the isobar in the nucleus, collision broadening will tend to increase the Δ width. This effect has been neglected in our calculations to date. We have estimated this effect by adding a constant collision width Γ_A to the isobar. The solid curve in Fig. 13(c) corresponds to $\Gamma_A=0$; the dashed curve corresponds to $\Gamma_A=30$ MeV. For the values we have chosen, the Pauli effect and collision broadening almost exactly compensate one another, e.g., compare Figs. 13(b) and 13(c). This suggests that we have overestimated the magnitude of the Pauli effects since isobar-hole calculations [8] predict a net increase in the Δ width in medium due to nuclear effects. However, our crude estimates suggest that the energy and angle dependence of the resulting cross sections will not change much when collision broadening is included.

In our model we have approximated the isobar-nucleus interaction in terms of an effective interaction which is

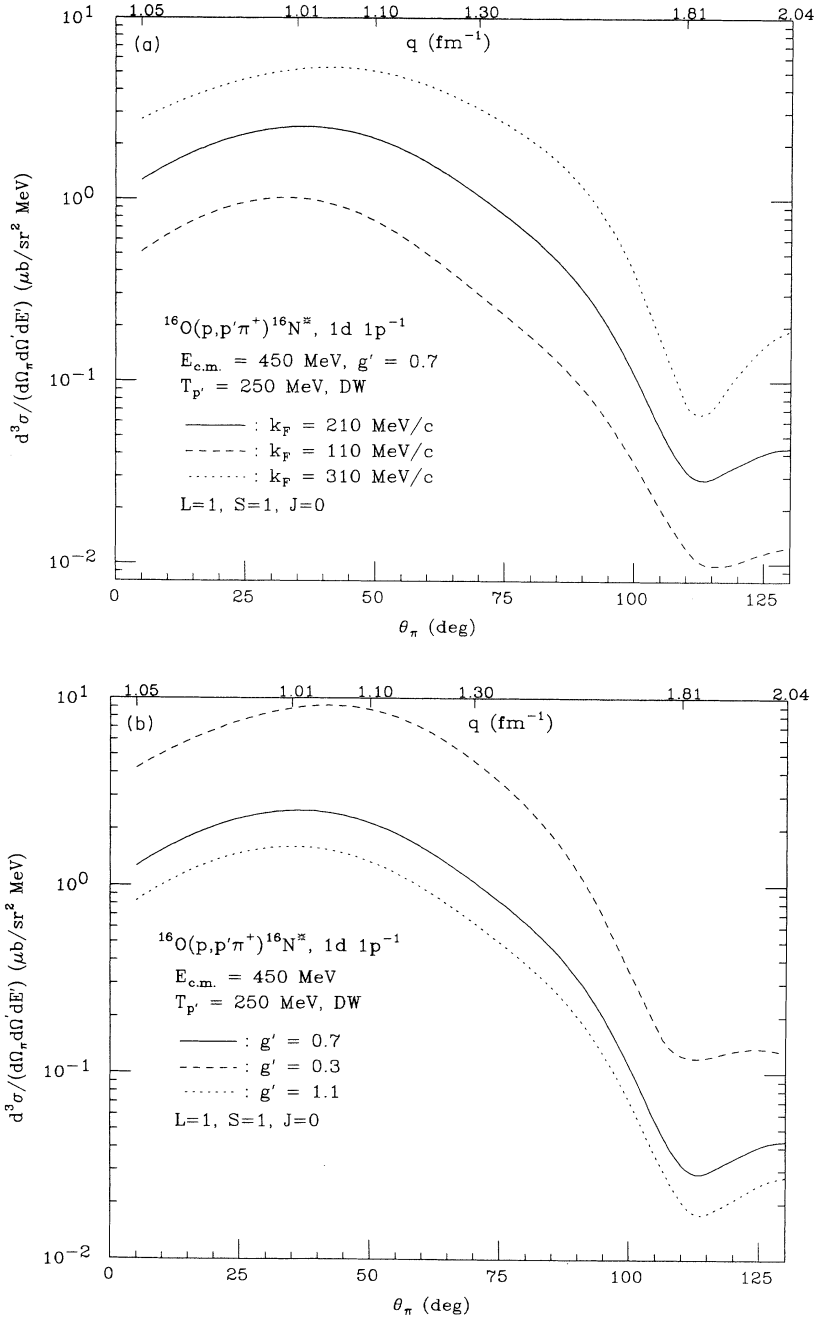

FIG. 11. Dependence of reaction cross sections on parameters chosen for pion self-energy. Distorted-wave differential cross section vs outgoing pion angle, including only amplitude A'_1. (a) Dependence on effective Fermi momentum k_F. Solid curve: $k_F=210$ MeV/c; dashed curve: $k_F=110$ MeV/c; dotted curve: $k_F=310$ MeV/c. (b) Dependence of reaction cross sections on value chosen for Landau-Migdal parameter for baryon-baryon short-range repulsion. Solid curve: $g'=0.7$; dashed curve: $g'=0.3$; dotted curve: $g'=1.1$.

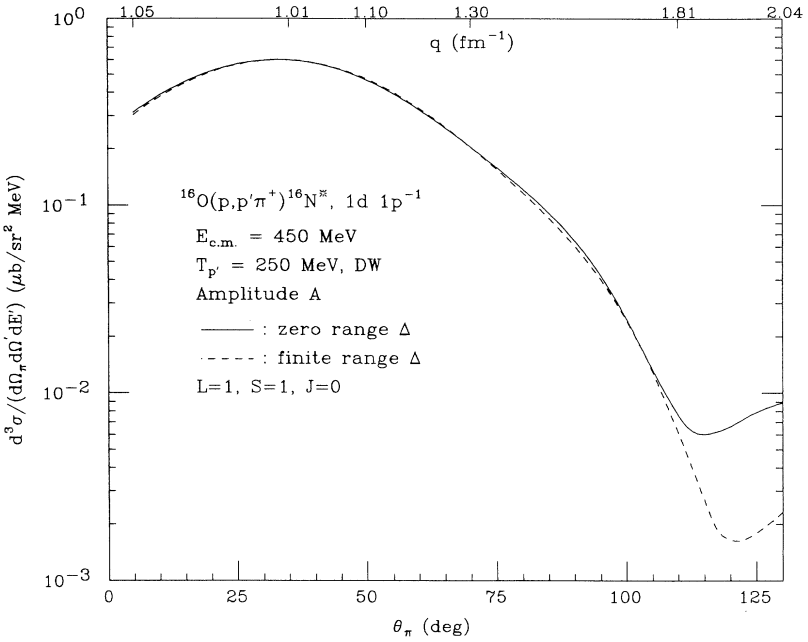

FIG. 12. Dependence of reaction cross sections on finite range for Δ propagation. Distorted-wave differential cross section as a function of outgoing pion angle for transition to $(1d)(1p)^{-1}$, $L=1$, $S=1$, $J=0$ final nuclear state, using amplitude A_1' only. Solid curve: zero-range approximation used for Δ propagation; dashed curve: finite-range calculation of Δ propagation.

the same for all intermediate states. This differs from the isobar-hole model [7,8,16] where the nuclear Hamiltonian is diagonalized to find isobar-doorway states. In such calculations the resulting effective interaction of the isobar is state dependent. Although our model gives a realistic average nuclear interaction for the isobar, there are some aspects of pion scattering for which this state dependence is quite important [8]. In subsequent calculations more reliable results could be obtained by replacing our isobar term by a sum over the dominant isobar-hole states in this reaction.

In our numerical calculations we have approximated the proton and pion distorted wave functions for a given angular momentum as a sum over spherical Bessel functions. Having chosen the number of basis states and the dispersion in momenta (as discussed in Sec. II), the expansion coefficients are obtained by fitting exact and approximate wave functions from the origin out to 15 fm for the protons, and out to 10 fm for the pion. It is important to test the validity of this approximation. As one test of this method, we vary the matching radius, refit the Bessel function expansion, and recalculate reaction cross sections. We apply this to model calculations containing only amplitude D_1' of Fig. 1(d), which should be the amplitude most sensitive to this fitting procedure. Radial integrals involving amplitudes B_1' and C_1' converge rapidly

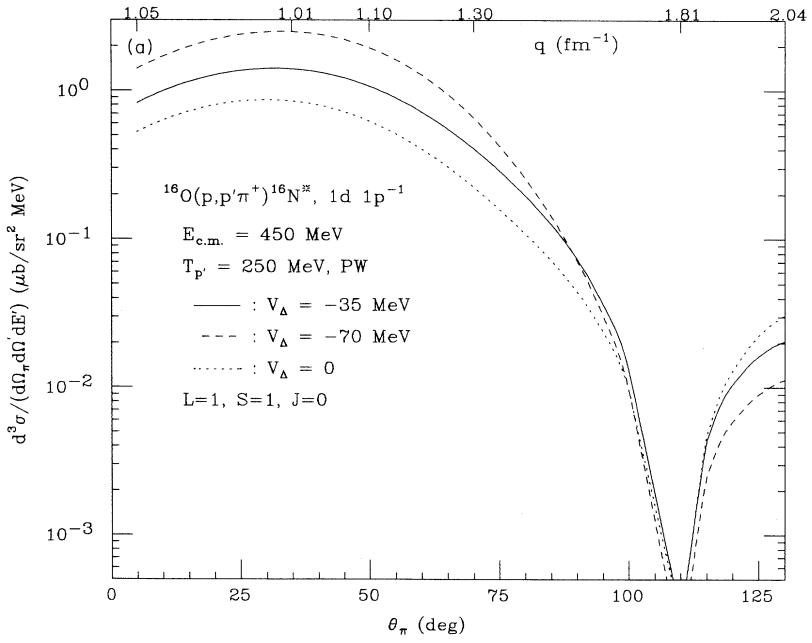

FIG. 13. Dependence of reaction cross sections on parametrization of Δ-nucleus interaction. Differential cross section as a function of outgoing pion angle for transition to $(1d)(1p)^{-1}$, $L=1$, $S=1$, $J=0$ final nuclear state in plane-wave approximation, using amplitude A_1 only. (a) Dependence on real part of Δ-nucleus interaction; assumed constant shift $\mathcal{V}_\Delta$. Dotted curve: $\mathcal{V}_\Delta=0$; solid curve: $\mathcal{V}_\Delta=-35$ MeV; dashed curve: $\mathcal{V}_\Delta=-70$ MeV. (b) Dependence of reaction cross sections on isobar width in nuclear medium. Pauli principle corrections to isobar width. Solid curve: Pauli factor $P=1$ [see Eq. (2.7)]; dashed curve: Pauli factor $P=0.7$. (c) Effects of isobar-nucleus spreading width. Solid curve: $\Gamma_A=0$ [see Eq. (2.7)]; dashed curve: $\Gamma_A=30$ MeV.

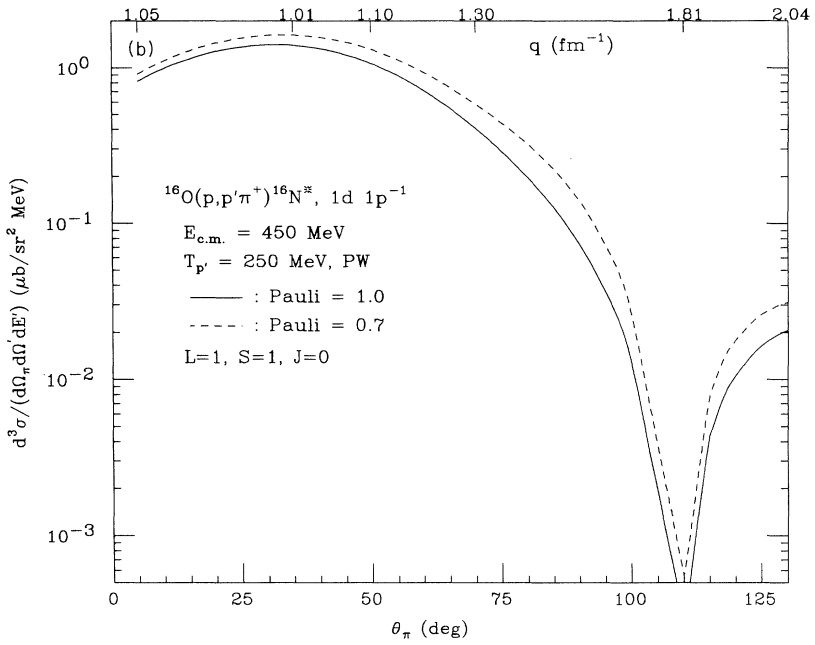

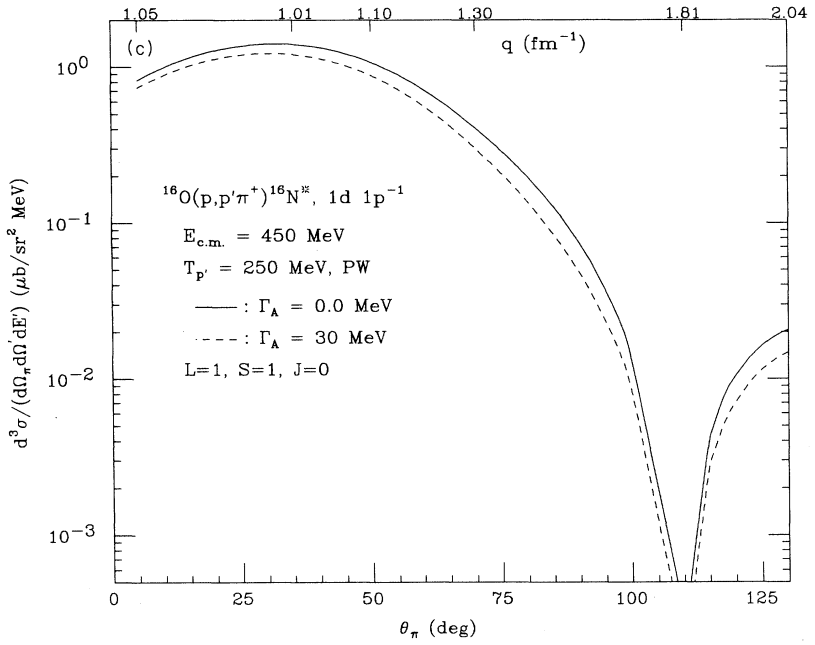

FIG. 13. (*Continued*).

because of the presence of bound-state wave functions, as can be seen by comparing Eqs. (A1) and (A3) with (A5). For amplitude A_1, the radial integrals involve creation of a virtual pion at one point inside the nucleus and destruction of the meson at another point. Distorted waves for the incident and final hadrons are modulated by nuclear transition densities. Therefore, relative to the center of the nucleus, our approximation for the distorted waves is only relevant where the nuclear transition density is non-negligible. The matching radii for the Bessel function expansions of our distorted waves are chosen to satisfy this condition.

The three curves in Fig. 14 show calculated cross sections for amplitude D_1' as the matching radius R is varied from 15 to 17 fm. Cross sections are calculated to a state with $L=S=1$ and $J=2$. The cross sections are virtually unchanged except at the deep minima in the cross section. This suggests that expansion of our distorted waves in a basis of spherical Bessel functions is not a source of considerable uncertainty in our calculated results.

In the next section we further discuss the implications of the results summarized above, and suggest future experimental and theoretical work on the $(N,N'\pi)$ reaction.

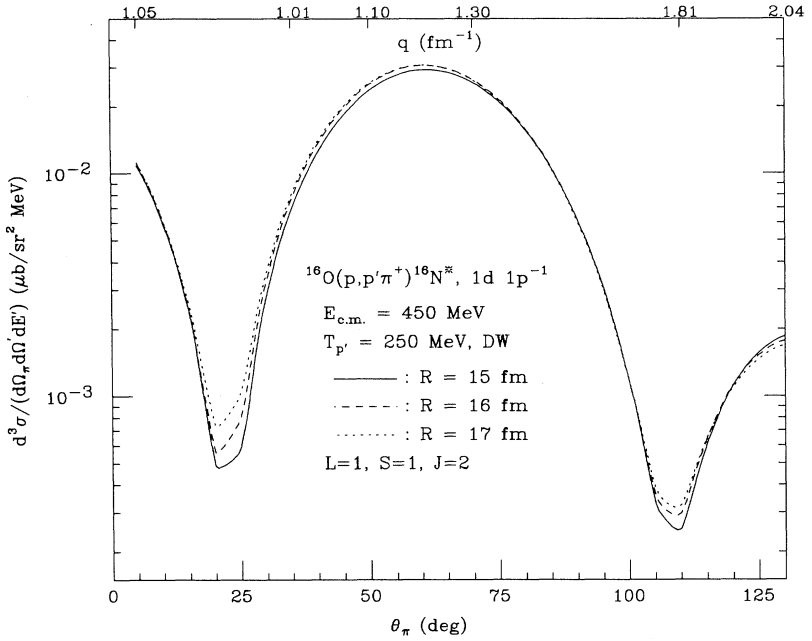

FIG. 14. Dependence of reaction cross sections on spherical Bessel function approximation to distorted-wave functions. Distorted-wave differential cross section as a function of outgoing pion angle for transition to $(1d)(1p)^{-1}$, $L=1$, $S=1$, $J=2$ final nuclear state, using amplitude D_1' only. Distorted waves for protons are expanded in a spherical Bessel function basis as given in Eq. (2.18). Expansion coefficients are obtained by least-squares fit of approximate wave function to the distorted wave function from the origin out to some distance R. Solid curve: cross section when $R=15$ fm; dashed curve: $R=16$ fm; dotted curve: $R=17$ fm.

IV. SUMMARY AND CONCLUSIONS

In this paper we have presented a two-nucleon model to describe the exclusive $(N,N'\pi)$ reaction. The model is applied in a region which should be dominated by formation of an intermediate $\Delta(1232)$ isobar. The reaction is assumed to proceed by exciting a nucleon to an isobar, which propagates and then decays to nucleon plus pion. Antisymmetrizing this amplitude with respect to both initial- and final-state nucleons leads to four distinct amplitudes, which are shown schematically in Fig. 1. These "postemission" amplitudes produce the pion at the isobar decay vertex. Four additional amplitudes, shown in Fig. 2, result when the pion is produced at the isobar formation vertex.

The resulting eight amplitudes have been calculated and applied to the $(p,p'\pi^+)$ reaction on ^{16}O leading to one-particle–one-hole states in ^{16}N. Differential cross sections to these states were obtained in a distorted-wave calculation using the dominant postemission amplitudes. The four preemission amplitudes were shown to be negligible in plane-wave approximation, because of adverse isospin coupling coefficients, and also because the Δ propagator in preemission amplitudes is far off shell at these energies. We expect the same results in distorted wave calculations.

The calculations shown in this paper assumed exchange of a virtual pion between active nucleons in the hard scattering process $NN\rightarrow NN\pi$. We also calculated the contribution for an intermediate ρ meson in addition to the intermediate pion. At low momentum transfers $q\leq 1$ fm^{-1} the contribution from ρ exchange is insignificant, but at higher momentum transfers the ρ meson contribution can become quite important. This amplitude should be included in subsequent calculations of this process, which involve large momentum transfers to the nucleus.

We are encouraged by the promising development of experimental techniques that now allow coincidence experiments to be performed with high-energy resolution (≈ 1 MeV) at high beam intensity (≈ 10 nA). Given a typical Indiana University Cyclotron Facility (IUCF) or TRIUMF target thickness of 50 mg/cm^2, and with cross-section magnitudes predicted here (≈ 1 μb/sr^2 MeV), one can expect to measure counts on the order of 1 count/min MeV. Thus the predicted strengths of the possible transitions make it feasible to experimentally measure and isolate some of the dominant transitions.

The spin-isospin selectivity provided by the nuclear response allows one in principle to isolate individual amplitudes in this reaction. For example, Fig. 5(b) shows that the 15 MeV 3^- normal parity transition is completely dominated by amplitude B_1' of Eq. (2.2). Provided one could experimentally extract the reaction cross section leading to this state, measurement of this transition would allow one to isolate and study amplitude B_1'.

The results of our calculation depend on values assumed for the medium dependence of both mesons and isobars. These have been parametrized in terms of effective widths and potentials, form factors, and other parameters, for which we have taken values consistent with other theoretical investigations in the same energy and momentum transfer regime. We investigated the sensitivity of our results to variation of these parameters; this should provide some "theoretical error bars" of inherent uncertainties in our calculations. For example, we used a zero-range approximation for the Δ in our calculation. Removing this approximation makes small changes in the calculated cross sections except in the vicinity of a deep minimum in the theoretical results.

We also showed the dependence of our results on the parameters used to define nuclear effects in Δ propaga-

tion, the intermediate pion self-energy, and the hadronic form factors. In some cases our cross sections are extremely sensitive to these assumptions. In particular, the cross sections appear to be highly sensitive to the form of the pion self-energy, at least for one of the reaction amplitudes. While this amplitude contributes only to certain final nuclear states, the shape of excitation functions for such transitions might be sensitive to the form chosen for the pion self-energy. In fact, if we examine the cross sections to a particular final state (as a function of pion angle for fixed outgoing proton energy), the self-energy contributions tend to change the magnitude of these cross sections while leaving their shape invariant.

There are several advantages to the present proposed study of the $(p,p'\pi^+)$ reaction. We used nuclear wave functions whose momentum transfer dependence was obtained from inelastic electron scattering studies. Such wave functions are realistic for momentum transfers $q \leq 200$ MeV/c, so our angular distributions should be most reliable in this kinematic region. One minimizes the uncertainties in the distorted wave functions (obtained from proton- and pion-nucleus scattering data) by working in an energy regime for which the distortion effects are small (200–500 MeV for protons and 50–100 MeV for the pion). We assumed the reaction could be described by a single hard scattering modulated by nuclear (optical) distortions of the outgoing particles; this assumption could be invalid if the reaction proceeds via multistep direct processes. If that is the case, then our theoretical cross sections would not fit either the magnitude or shape of the experimental results. However, it is reasonable to expect that the model is adequate (at least in this energy-momentum regime) so that it can provide a theoretical guide for interpreting the data. Of course, there are sufficiently many degrees of freedom in this calculation that quantitative prediction of cross sections to individual states may not be feasible. We are currently examining processes where one could extract information about individual amplitudes and contributions by comparing transitions to different final states, or to the same final state at different momentum transfers. Our results suggest such comparisons may be much less sensitive to theoretical uncertainties. We are also investigating ways to extract useful information in this reaction even in the presence of substantial experimental backgrounds.

We observed earlier that amplitude A_1 shows a strong dependence on the form of the self-energy of the intermediate pion. Amplitudes which have no contribution from this term (e.g., normal parity transitions) are only weakly affected by the self-energy term, while in our model abnormal parity $T=1$ states should be increased by factors of 5–10. Comparison of experimental strength to normal parity states with cross sections to abnormal parity $T=1$ states should show directly whether our predicted enhancement is present. Another test of our predictions is to take ratios of the same isobaric transition for different $(N,N'\pi)$ isospin channels, i.e., the cross section ratio of $(p,p'\pi^+)$ to $(p,n\pi^+)$, in transitions to nuclear states with $T=1$.

We continue to study the theoretical cross sections as a function of nuclear momentum transfer and energy. It may be possible to extract individual amplitudes in much the same way that the Rosenbluth plot has been useful in electron scattering [29, 30]. Siciliano and Walker [31] have previously discussed the promise of such techniques in hadronic interactions. If the (q,E) separation predicted by our calculations is not confirmed experimentally, this would provide strong evidence that the reaction proceeds through a more complex mechanism.

The goal of this present study is to isolate those features of the model which fix the qualitative behavior of reaction cross sections in this kinematic region. If the reaction mechanism is shown to be adequate from such combined theoretical-experimental studies, then one can hope to investigate other interesting features associated with the $(N,N'\pi)$ reaction such as the nuclear response at higher momentum transfer and the description of meson and baryon propagation in nuclei.

ACKNOWLEDGMENTS

This research was supported in part by the U.S. National Science Foundation under Contract No. NSF-PHY91-08036. The authors wish to thank R. D. Bent, B. K. Jain, L. C. Liu, and E. R. Siciliano for discussions and suggestions regarding this problem.

APPENDIX A: AMPLITUDES B'_1, C'_1, AND D'_1, IN DISTORTED-WAVE APPROXIMATION

1. Amplitude B'_1

The amplitude B'_1 shown in Fig. 1(b) represents the post-emission exchange target excitation process; i.e., an amplitude where a target nucleon is excited to a Δ, which propagates and then decays to the final continuum proton and pion, while the incident proton is captured into a particle-hole final nuclear state. When we remove the overall Clebsch-Gordan angular momentum coefficients [cf. Eq. (2.28)], the expression for B'_1 has the form

$$B'_1=(-1)^{l_h+J}64\sqrt{6\pi}\hat{l}_p\hat{l}_h\hat{L}\hat{S}\hat{J}\hat{S}'\frac{B_1^I}{D_\Delta(q_B^\Delta,\omega_B^\Delta)}$$
$$\times\sum_{l_1,\ldots,l_8 l_{12},L_3 S_2,S_4 i,j,\epsilon}\alpha_{l_1,i}\beta_{l_2,j}\gamma_{l_3,\epsilon}q'_\epsilon(-1)^{l_8+l_9+l_{12}}(i)^{-l_1-l_2+L_3-l_4-l_5+1}$$
$$\times\hat{l}_1\hat{l}_2\hat{l}_3\hat{L}_3\hat{l}_4\hat{l}_5^2\hat{l}_8\hat{l}_{12}^2\hat{S}_2^2\hat{S}_4^2C_{0\,0\,0}^{1\,l_3\,L_3}C_{0\,0\,0}^{l_4\,l_5\,l_7}C_{000}^{1\,1\,l_7}$$
$$\times\{[Y^{l_1}(\hat{\mathbf{k}})\otimes Y^{l_2}(\hat{\mathbf{k}}')]^{l_8}\otimes Y^{l_3}(\hat{\mathbf{q}}')\}_{m_9}^{l_9}$$

$$\times \begin{Bmatrix} \frac{1}{2} & 1 & \frac{3}{2} \\ 1 & \frac{1}{2} & S_2 \end{Bmatrix} \begin{Bmatrix} L & J & S \\ S' & S_4 & l_9 \end{Bmatrix} \begin{Bmatrix} l_{12} & l_8 & L_3 \\ l_3 & 1 & l_9 \end{Bmatrix} \begin{Bmatrix} l_7 & L & l_{12} \\ l_9 & 1 & S_4 \end{Bmatrix}$$

$$\times \begin{Bmatrix} S_4 & 1 & l_7 \\ 1 & 1 & S_2 \end{Bmatrix} \begin{Bmatrix} l_2 & L_3 & l_6 \\ l_{12} & l_1 & l_8 \end{Bmatrix} \begin{Bmatrix} \frac{1}{2} & \frac{1}{2} & S \\ 1 & S_2 & S_4 \\ \frac{1}{2} & \frac{1}{2} & S' \end{Bmatrix} \begin{Bmatrix} l_6 & l_5 & l_h \\ l_1 & l_4 & l_p \\ l_{12} & l_7 & L \end{Bmatrix}$$

$$\times \int_0^\infty dq \, \frac{q^4 f(q)}{D_\pi(q,\omega_B)} \left[C_{0\,0\,0}^{l_1 l_p l_4} \int_0^\infty r_1^2 dr_1 j_{l_1}(k_i r_1) j_{l_4}(qr_1) R_{l_p}^{n*}(r_1) \right]$$

$$\times \left[C_{0\,0\,0}^{l_2 L_3 l_6} C_{0\,0\,0}^{l_5 l_h l_6} \int_0^\infty r_2^2 dr_2 j_{l_2}(k_j' r_2) j_{L_3}(q'_\epsilon r_2) j_{l_5}(qr_2) R_{l_h}^{n'}(r_2) \right] . \tag{A1}$$

The coordinate radial integrals all involve products of three spherical Bessel functions, or two Bessel functions times a harmonic-oscillator wave function, and hence can be evaluated analytically [17]. The nuclear isospin factor B_1^I has the form

$$B_1^I = -\sqrt{2}(-1)^{T_z} C_{t_{z_f}}^{1/2\,1\,3/2}{}_{\lambda' t_{z_\Delta}} \times C_{-t_{z_i}}^{1/2\,1\,3/2}{}_{T_z - t_{z_\Delta}} (\hat{\phi}'\dagger)_{\lambda'} \delta_{T,1} , \tag{A2}$$

which has the value $B_1^I = \sqrt{2}\delta_{T,1}$ for the $(p,p'\pi^+)$ process. Isospin conservation requires that this amplitude excite only $T=1$ final states for an initial state with $T=0$.

2. Amplitude C_1'

The amplitude C_1', shown in Fig. 1(c), is the postemission exchange projectile excitation term. This term is obtained from Fig. 1(a) by interchanging the two final-state nucleons. It represents the hard scattering amplitude where the projectile nucleon is excited to an isobar which then decays to a bound nucleon and free pion; the initially bound nucleon which participates in the hard scattering is ejected in the final continuum state. When the angular momentum Clebsch-Gordan factor is removed the reduced amplitude C_1' may be written as

$$C_1' = (-1)^{l_h + L + J} 64\sqrt{6\pi} \hat{l}_p \hat{l}_h \hat{L} \hat{S} \hat{J} \hat{S}' \frac{C_1^I}{D_\Delta(q_C^\Delta, \omega_C^\Delta)}$$

$$\times \sum_{l_1,\ldots,l_8 l_{12}, L_3 S_2, S_4 i,j,\epsilon} \sum \sum \sum \alpha_{l_1,i} \beta_{l_2,j} \gamma_{l_3,\epsilon} q'_\epsilon (-1)^{l_9 + l_{12} + S_4 + 1} (i)^{l_1 - l_2 - L_3 + l_5 - l_6 - 1}$$

$$\times \hat{l}_1 \hat{l}_3 \hat{L}_3 \hat{l}_5^2 \hat{l}_6^2 \hat{l}_8 \hat{l}_{12}^2 \hat{S}_2^2 \hat{S}_4^2 C_{0\,0\,0}^{1\,l_3 L_3} C_{0\,0\,0}^{l_5 l_6 l_7} C_{0\,0\,0}^{1\,1\,l_7} \{ [Y^{l_1}(\hat{\mathbf{k}}) \otimes Y^{l_2}(\hat{\mathbf{k}}')]^{l_8} \otimes Y^{l_3}(\hat{\mathbf{q}}') \}_{m_9}^{l_9}$$

$$\times \begin{Bmatrix} \frac{1}{2} & 1 & \frac{3}{2} \\ 1 & \frac{1}{2} & S_2 \end{Bmatrix} \begin{Bmatrix} L & J & S \\ S' & S_4 & l_9 \end{Bmatrix} \begin{Bmatrix} l_{12} & l_8 & L_3 \\ l_3 & 1 & l_9 \end{Bmatrix} \begin{Bmatrix} l_7 & L & l_{12} \\ l_9 & 1 & S_4 \end{Bmatrix}$$

$$\times \begin{Bmatrix} S_4 & 1 & l_7 \\ 1 & 1 & S_2 \end{Bmatrix} \begin{Bmatrix} L_3 & l_1 & l_4 \\ l_2 & l_{12} & l_8 \end{Bmatrix} \begin{Bmatrix} \frac{1}{2} & \frac{1}{2} & S \\ S_2 & 1 & S_4 \\ \frac{1}{2} & \frac{1}{2} & S' \end{Bmatrix} \begin{Bmatrix} l_{12} & l_2 & l_4 \\ L & l_h & l_p \\ l_7 & l_6 & l_5 \end{Bmatrix}$$

$$\times \int_0^\infty dq \frac{q^4 f(q)}{D_\pi(q,\omega_C)} \left[C_{0\,0\,0}^{l_6 l_h l_2} \int_0^\infty r_1^2 dr_1 j_{l_2}(k_j' r_1) j_{l_6}(qr_1) R_{l_h}^{n'}(r_1) \right]$$

$$\times \left[C_{0\,0\,0}^{l_5 l_p l_4} C_{0\,0\,0}^{l_1 L_3 l_4} \int_0^\infty r_2^2 dr_2 j_{l_5}(qr_2) R_{l_p}^{n*}(r_2) j_{l_1}(k_i r_2) j_{L_3}(q'_\epsilon r_2) \right] , \tag{A3}$$

The isospin factor, C_1^I in Eq. (A3) is given by

$$C_1^I = 2\sqrt{6}(-1)^{1/2 - t_{z_h} + \lambda} C_{t_{z_p}}^{1/2\,1/2\,T}{}_{-t_{z_h} T_z} C_{-t_{z_f}}^{1/2\,1\,1/2}{}_{\lambda - t_{z_h}} \times \sum_T' \hat{T}' C_{-t_{z_p}}^{1/2\,T'\,1/2}{}_{T'_z - t_{z_i}} C_{-\lambda' - \lambda T'_z}^{1\,1\,T'} \begin{Bmatrix} \frac{1}{2} & 1 & \frac{3}{2} \\ 1 & \frac{1}{2} & T' \end{Bmatrix} (\hat{\phi}'\dagger)_{\lambda'} , \tag{A4}$$

which has the value of $-\sqrt{2/3}$ for the $(p,p'\pi^+)$ reaction.

3. Amplitude D_1'

The amplitude D_1', shown schematically in Fig. 1(d), is the postemission direct target excitation term. In this amplitude a target nucleon is excited to an isobar which decays to the final pion and a bound nucleon; the projectile interacts with the virtual meson and produces the final continuum proton. The expression for the reduced amplitude D_1' may be written as

$$D_1'=(-1)^{l_p+S+J}64\sqrt{2\pi}\hat{l}_p\hat{l}_h\hat{L}\hat{S}\hat{J}\delta_{S',1}\begin{Bmatrix}\frac{1}{2} & 1 & \frac{3}{2}\\ 1 & \frac{1}{2} & S\end{Bmatrix}\frac{D_1^I}{D_\Delta(q_D^\Delta,\omega_D^\Delta)}$$

$$\times\sum_{l_1,\ldots,l_5L_3,l_8}\sum_{i,j,\epsilon}\alpha_{l_1,i}\beta_{l_2,j}\gamma_{l_3,\epsilon}q_\epsilon'(i)^{l_1-l_2-L_3+l_4-l_8-1}\frac{\hat{l}_1\hat{l}_2\hat{l}_3\hat{L}_3\hat{l}_4^2\hat{l}_5}{\hat{l}_8}C_{0\,0\,0}^{l_1\,l_3\,L_3}C_{0\,0\,0}^{1\,l_4\,l_5}C_{0\,0\,0}^{1\,l_5\,l_8}$$

$$\times\{[Y^{l_1}(\hat{\mathbf{k}})\otimes Y^{l_2}(\hat{\mathbf{k}}')]^{l_8}\otimes Y^{l_3}(\hat{\mathbf{q}}')\}_{m_9}^{l_9}\begin{Bmatrix}1 & l_8 & l_5\\ l_3 & J & l_9\end{Bmatrix}\begin{Bmatrix}L & S & J\\ L_3 & 1 & l_3\\ l_4 & 1 & l_5\end{Bmatrix}$$

$$\times\int_{|k_i-k_j'|}^{k_i+k_j'}dq\frac{q^4f(q)}{D_\pi(q,\omega_D)}\left[C_{0\,0\,0}^{l_1\,l_2\,l_8}\int_0^\infty r_1^2dr_1j_{l_1}(k_ir_1)j_{l_2}(k_j'r_1)j_{l_8}(qr_1)\right]$$

$$\times\left[C_{0\,0\,0}^{L_3\,l_4\,L}C_{0\,0\,0}^{l_p\,l_h\,L}\int_0^\infty r_2^2dr_2j_{L_3}(q_\epsilon'r_2)j_{l_4}(qr_2)R_{l_p}^{n*}(r_2)R_{l_h}^{n'}(r_2)\right]. \tag{A5}$$

As with the other amplitudes, all coordinate space radial integrals in Eq. (A5) can be done analytically. The resulting isospin factor D_1^I is given by

$$D_1^I=4\sqrt{2}(-1)^{\lambda'+t_{z_f}+1/2}C_{t_{z_i}\,-t_{z_f}}^{1/2\,1/2\,\,1}C_{\lambda'\,-\lambda\,-T_z}^{1\,1\,\,T}\times\begin{Bmatrix}\frac{1}{2} & 1 & \frac{3}{2}\\ 1 & \frac{1}{2} & T\end{Bmatrix}(\hat{\phi}'^\dagger)_{\lambda'}, \tag{A6}$$

and has the value of $-\sqrt{2/3}$ for $(p,p'\pi^+)$. Note that, using conservation of parity and angular momentum, the amplitude D_1' cannot excite a $J=0$ final state when the initial closed-shell nucleus has $J=0$.

APPENDIX B: POSTEMISSION AMPLITUDES $\tilde{A}_1$, $\tilde{B}_1$, $\tilde{C}_1$ AND $\tilde{D}_1$ IN PLANE-WAVE APPROXIMATION

1. Amplitude $\tilde{A}_1$

In this paper we derived distorted-wave expressions for the exclusive $(N,N'\pi)$ process. It is useful to present plane-wave expressions for this process, for two reasons. First, plane-wave results have been obtained previously by Jain, Londergan, and Walker [14]; in plane-wave approximation many of the resulting integrals can be done analytically. In the present calculation the wave functions are decomposed into individual angular momentum states. If the distorted wave functions for each angular momentum are replaced by spherical Bessel functions then an independent check can be made of the plane wave results. Second, as we expanded all distorted waves in a plane-wave basis, the plane-wave results provide a check for our distorted-wave calculations. In this subsection we derive plane-wave results for the direct projectile excitation term.

Replacing the scattering wave functions in Eq. (2.24) by plane waves, the resulting delta functions fix the momenta of the intermediate pion, $\mathbf{q}_A$, and delta, $\mathbf{q}_A^\Delta$,

$$\mathbf{q}_A=\mathbf{k}'+\mathbf{q}'-\mathbf{k}, \tag{B1}$$

$$\mathbf{q}_A^\Delta=\mathbf{k}'+\mathbf{q}'. \tag{B2}$$

As was done in Sec. II, we extract a common factor

$$(-1)^{1/2-s_{z_f}}C_{s_{z_f}\,-s_{z_f}\,S_z'}^{1/2\,1/2\,\,S'}$$

from every amplitude. When we square these amplitudes, sum over angular momenta and use the orthogonality of the Clebsch-Gordan coefficients, the expression in Eq. (2.29) can be replaced by an equivalent expression for the reduced amplitudes,

$$\frac{1}{2}\sum_{S',S_z'}\sum_{J_z}|\tilde{A}_1-\tilde{B}_1-\tilde{C}_1+\tilde{D}_1|^2. \tag{B3}$$

We write the reduced amplitude $\tilde{A}_1$ as the product of three factors,

$$\tilde{A}_1\equiv A_1^IA_1^aA_1^b, \tag{B4}$$

where A_1^I is defined in Eq. (2.25), and where we define the quantities

$$A_1^a=(-1)^{l_h}i^L\sqrt{3}\frac{\hat{l}_p\hat{l}_h}{\hat{J}}\frac{f_{\pi NN}f_{\pi N\Delta}^2}{m_\pi^3}C_{0\,0\,0}^{l_p\,l_h\,L}C_{0\,0\,0}^{L\,1\,J}\times A_{l_p,l_h,L}^{n,n'}(q_A)Y_{J_z}^{J*}(\hat{\mathbf{q}}_A)\frac{F_A^\pi(q_A)}{D_\pi(q_A,\omega_A)D_\Delta(q_A^\Delta,\omega_A^\Delta)} \tag{B5}$$

and

$$A_1^b=-2(8\pi/3)^{3/2}q'q_A^2[Y^1(\hat{\mathbf{q}}')\otimes Y^1(\hat{\mathbf{q}}_A)]_{S_z'}^{S'}\times\begin{Bmatrix}1 & 1 & S'\\ \frac{1}{2} & \frac{1}{2} & \frac{3}{2}\end{Bmatrix}\delta_{S,1}, \tag{B6}$$

where the particle-hole matrix elements $A_{l_p,l_h,L}^{n,n'}$ are defined in Eq. (2.35). Since we are using harmonic-oscillator nuclear basis states, we can evaluate analytically the particle-hole matrix element integral; using the results of Ref. [30] we obtain

$$A^{n,n'}_{l_p,l_h,L}(q_A)=\frac{2^L}{(2L+1)!!}\sqrt{(n-1)!(n'-1)!\Gamma(n+l_p+\tfrac{1}{2})\Gamma(n'+l_h+\tfrac{1}{2})}(q_A/2p_0)^2$$
$$\times\exp\left[-\frac{q_A^2}{4p_0^2}\right]\sum_{m=0}^{n-1}\sum_{m'=0}^{n'-1}\frac{(-1)^{m+m'}}{m!m'!}\frac{1}{(n-m-1)!(n'-m'-1)!}\frac{\Gamma[\frac{1}{2}(l_p+l_h+2m+2m'+L+3)]}{\Gamma(m+l_p+\frac{3}{2})\Gamma(m'+l_h+\frac{3}{2})}$$
$$\times F\left[\frac{1}{2}(L-l_p-l_h-2m-2m');L+\frac{3}{2};\left[\frac{q_A}{2p_0}\right]^2\right], \tag{B7}$$

where $p_0=1/b$, b is the harmonic-oscillator length parameter chosen to be 1.77 fm [23]. $F(\alpha;\beta;y)$ is the confluent hypergeometric function given by

$$F(\alpha;\beta;y)=1+\frac{\alpha}{\beta}y+\frac{\alpha(\alpha+1)}{\beta(\beta+1)}\frac{y^2}{2!}+\cdots. \tag{B8}$$

For a nonpositive integer α the series appearing in Eq. (B8) terminates and $F(\alpha;\beta;y)$ is a polynomial of degree $-\alpha$ in y. For the calculations in this paper, the series terminates; for the particle-hole states we consider the overlap integrals $A^{n,n'}_{l_p,l_h,L}(q_A)$ take the following forms:

$$A^{1,1}_{2,1,1}(q_A)=\frac{1}{\sqrt{360}}\left[\frac{q_A}{p_0}\right]\left[10-\left[\frac{q_A}{p_0}\right]^2\right]\exp\left[-\frac{q_A^2}{4p_0^2}\right],$$
$$A^{1,1}_{2,1,3}(q_A)=\frac{1}{\sqrt{360}}\left[\frac{q_A}{p_0}\right]^3\exp\left[-\frac{q_A^2}{4p_0^2}\right], \tag{B9}$$
$$A^{2,1}_{0,1,1}(q_A)=-\frac{1}{12}\left[\frac{q_A}{p_0}\right]\left[4-\left[\frac{q_A}{p_0}\right]^2\right]\exp\left[-\frac{q_A^2}{4p_0^2}\right].$$

2. Amplitude $\tilde{B}_1$

To obtain plane-wave results for the exchange target excitation amplitude, we again write the reduced amplitude $\tilde{B}_1$ in expression (B3) as the product of three terms,

$$\tilde{B}_1\equiv B_1^I\sum_{t_1,t_2,m_2}B_{1a}(t_1,t_2,m_2)B_{1b}(t_1,t_2,m_2), \tag{B10}$$

where B_1^I is defined in Eq. (A2). The expression for $B_{1a}(t_1,t_2,m_2)$ is calculated separately for the different nuclear basis states, due to the complication of the expression. For the $1d(1p)^{-1}$ basis state we obtain

$$B_{1a}^{(1l_p)(1l_h)^{-1}}(t_1,t_2,m_2)$$
$$=8\pi\frac{f_{\pi NN}f^2_{\pi N\Delta}}{m_\pi^3}\frac{i^{l_p+l_h}}{p_0^{l_p+l_h+3}}\frac{\hat{l}_p\hat{l}_h\hat{L}\hat{J}}{\sqrt{\Gamma(l_p+\frac{3}{2})\Gamma(l_h+\frac{3}{2})}}\frac{\exp[-(k^2+|\mathbf{k}'+\mathbf{q}'|^2)/2p_0^2]}{D_\Delta(q_B^\Delta,\omega_B^\Delta)}$$
$$\times\sum_{l_1=0}^{l_p}\sum_{l_2=0}^{l_h}\sum_{l_3,\ldots,l_6}\sum_{m_5}(-1)^{l_4+l_6+L+J+J_z}\begin{bmatrix}2l_p+1\\2l_1\end{bmatrix}^{1/2}\begin{bmatrix}2l_h+1\\2l_2\end{bmatrix}^{1/2}\hat{l}_3\hat{l}_4\hat{l}_6k^{l_p-l_1}|\mathbf{k}'+\mathbf{q}'|^{l_h-l_2}$$
$$\times I_B(l_1,l_2,l_6)C^{l_1\,l_2\,l_3}_{0\,0\,0}C^{l_3\,l_6\,t_1}_{0\,0\,0}C^{J\;\;t_2\;\;l_5}_{-J_z\,m_2\,m_5}$$
$$\times\begin{Bmatrix}l_5&L&t_1\\S&t_2&J\end{Bmatrix}\begin{Bmatrix}L&l_4&l_3\\l_6&t_1&l_5\end{Bmatrix}\begin{Bmatrix}l_p&l_h&L\\l_p-l_1&l_h-l_2&l_4\\l_1&l_2&l_3\end{Bmatrix}\{[Y^{l_p-l_1}(\hat{\mathbf{k}})\otimes Y^{l_h-l_2}(\widehat{\mathbf{k}'+\mathbf{q}'})]^{l_4}\otimes Y^{l_6}(\hat{\mathbf{R}})\}^{l_5}_{m_5}, \tag{B11}$$

and for the $2s(1p)^{-1}$ state

$$B_{1a}^{(2s)(1p)^{-1}}(t_1,t_2,m_2)$$
$$=8i^L\frac{f_{\pi NN}f^2_{\pi N\Delta}}{m_\pi^3}\frac{\hat{L}\hat{J}}{p_0^{L+3}}(-1)^{L+J+J_z}\frac{\exp[-(k^2+|\mathbf{k}'+\mathbf{q}'|^2)/2p_0^2]}{D_\Delta(q_B^\Delta,\omega_B^\Delta)}$$
$$\times\sum_{l_2'=0}^{L}\sum_{l_5',m_5'}\sum_{l_6'}\hat{l}_6'\begin{bmatrix}2L+1\\2l_2'\end{bmatrix}^{1/2}|\mathbf{k}'+\mathbf{q}'|^{L-l_2'}C^{J\;\;t_2\;\;l_5'}_{-J_z\,m_2\,m_5'}\begin{Bmatrix}l_5'&L&t_1\\S&t_2&J\end{Bmatrix}$$

$$\times\left|(-1)^{t_1}I'_{B_1}(l'_2,l'_6)C^{l'_2\,l'_6\,t_1}_{0\,0\,0}[Y^{L-l'_2}(\mathbf{k}'+\hat{\mathbf{q}}')\otimes Y^{l'_6}(\hat{\mathbf{R}})]^{l'_5}_{m'_5}\begin{Bmatrix}L & L-l'_2 & l'_2\\ l'_6 & t_1 & l'_5\end{Bmatrix}\right.$$

$$\left.-(-1)^{l'_5}\frac{8\sqrt{3\pi}}{9p_0^2}kI'_{B_2}(l'_2,l'_6)\right.$$

$$\left.\times\sum_{l'_3,l'_4}\hat{l}'_3\hat{l}'_4C^{1\,l'_2\,l'_3}_{0\,0\,0}C^{l'_3\,l'_6\,t_1}_{0\,0\,0}\{[Y^{L-l'_2}(\widehat{\mathbf{k}'+\mathbf{q}'})\otimes Y^{l'_6}(\hat{\mathbf{R}})]^{l'_4}\otimes Y^1(\hat{\mathbf{k}})\}^{l'_5}_{m'_5}\begin{Bmatrix}L & t_1 & l'_5\\ L-l'_2 & l'_6 & l'_4\\ l'_2 & l'_3 & 1\end{Bmatrix}\right|. \quad \text{(B12)}$$

The expressions $\mathbf{R}$ and $I_B(l_1,l_2,l_6)$ are given by

$$\mathbf{R}\equiv\mathbf{k}+\mathbf{k}'+\mathbf{q}' , \quad \text{(B13)}$$

$$I_B(l_1,l_2,l_6)\equiv\int_0^\infty dq\frac{q^{l_1+l_2+4}}{D_\pi(q,\omega_B)}F_B^\pi(q)e^{-q^2/p_0^2}\times i_{l_6}(qR/p_0^2) , \quad \text{(B14)}$$

where $i_n(x)$ appearing in Eq. (B14) is the modified spherical Bessel function which is related to the modified Bessel function $I_n(x)$ [32] through

$$i_n(x)=(\pi/2x)^{1/2}I_{n+1/2}(x) .$$

In addition, we have

$$I'_{B_1}(l'_2,l'_6)\equiv\int_0^\infty dq\frac{q^{l'_2+4}[(2/3p_0^2)(q^2+k^2)-1]}{D_\pi(q,\omega_B)}\times F_B^\pi(q)e^{-q^2/p_0^2}i_{l'_6}(qR/p_0^2) , \quad \text{(B15)}$$

$$I'_{B_2}(l'_2,l'_6)\equiv\int_0^\infty dq\frac{q^{l'_2+5}}{D_\pi(q,\omega_B)}F_B^\pi(q)e^{-q^2/p_0^2}\times i_{l'_6}(qR/p_0^2) . \quad \text{(B16)}$$

We calculate the above integrals numerically using Gauss-Legendre quadrature for the integration points. The form of the final term, $B_{1b}(t_1,t_2,m_1)$, is independent of the nuclear basis state, so we obtain

$$B_{1b}(t_1,t_2,m_2)=16\pi\sqrt{2}q'\hat{S}\sum_{m_1}(-1)^{t_2}\hat{t}_2^2C^{1\,1\,t_1}_{0\,0\,0}C^{1\,\,t_2\,\,S'}_{m_1\,m_2\,S'_z}Y^1_{m_1}(\hat{\mathbf{q}}')\times\begin{Bmatrix}1 & t_2 & S'\\ \frac{1}{2} & \frac{1}{2} & \frac{3}{2}\end{Bmatrix}\begin{Bmatrix}1 & 1 & t_1\\ \frac{1}{2} & \frac{1}{2} & S\\ \frac{3}{2} & \frac{1}{2} & t_2\end{Bmatrix} . \quad \text{(B17)}$$

3. Amplitude $\tilde{C}_1$

All of the other postemission amplitudes impose spin and/or isospin selection rules on the final nuclear state (for reactions on a $T=0$ closed-shell target); however, there are no selection rules accompanying the amplitude C_1. To proceed, we write the reduced amplitude $\tilde{C}_1$ as the product of three terms, in analogy to Eq. (B10) for amplitude $\tilde{B}_1$. The isospin part, C_1^I, is given in Eq. (A4). Just as for amplitude $\tilde{B}_1$, we evaluate the term $C_{1a}(t_1,t_2,m_2)$ separately for the two basis states $(1d)(1p)^{-1}$ and $(2s)(1p)^{-1}$:

$$C_{1a}^{(1l_p)(1l_h)^{-1}}(t_1,t_2,m_2)=8\pi\frac{f_{\pi NN}f^2_{\pi N\Delta}}{m_\pi^3}\frac{i^{l_p+l_h}}{p_0^{l_p+l_h+3}}\frac{\hat{l}_p\hat{l}_h\hat{L}\hat{J}}{\sqrt{\Gamma(l_p+\frac{3}{2})\Gamma(l_h+\frac{3}{2})}}\frac{\exp[-(k'^2+|\mathbf{k}-\mathbf{q}'|^2)/2p_0^2]}{D_\Delta(q_C^\Delta,\omega_C^\Delta)}$$
$$\times\sum_{l_1=0}^{l_p}\sum_{l_2=0}^{l_h}\sum_{l_3,\ldots,l_6}\sum_{m_5}(-1)^{l_2+l_4+L+J+J_z}\begin{bmatrix}2l_p+1\\ 2l_2\end{bmatrix}^{1/2}\begin{bmatrix}2l_h+1\\ 2l_2\end{bmatrix}^{1/2}\hat{l}_3\hat{l}_4\hat{l}_6|\mathbf{q}'-\mathbf{k}|^{l_p-l_1}$$
$$\times k'^{l_h-l_2}I_C(l_1,l_2,l_6)C^{l_1\,l_2\,l_3}_{0\,0\,0}C^{l_3\,l_6\,t_1}_{0\,0\,0}C^{J\,\,t_2\,\,l_5}_{-J_z\,m_2\,m_5}$$
$$\times\begin{Bmatrix}l_5 & L & t_1\\ S & t_2 & J\end{Bmatrix}\begin{Bmatrix}L & l_4 & l_3\\ l_6 & t_1 & l_5\end{Bmatrix}\begin{Bmatrix}l_p & l_h & L\\ l_p-l_1 & l_h-l_2 & l_4\\ l_1 & l_2 & l_3\end{Bmatrix}$$
$$\times\{[Y^{l_p-l_1}(\widehat{\mathbf{q}'-\mathbf{k}})\otimes Y^{l_h-l_2}(\hat{\mathbf{k}}')]^{l_4}\otimes Y^{l_6}(\hat{\mathbf{R}}')\}^{l_5}_{m_5}, \quad \text{(B18)}$$

and

$$C_{1a}^{(2s)(1p)^{-1}}(t_1,t_2,m_2)$$

$$=8i^L\frac{f_{\pi NN}f_{\pi N\Delta}^2}{m_\pi^3}\frac{\hat{L}\hat{J}}{p_0^{L+3}}(-1)^{L+J+J_z}\frac{\exp[-(k'^2+|\mathbf{k}-\mathbf{q}'|^2)/2p_0^2]}{D_\Delta(q_C^\Delta,\omega_C^\Delta)}$$

$$\times\sum_{l_2'=0}^{L}\sum_{l_5',m_5'}\sum_{l_6'}(-1)^{l_2'+l_5'+l_6'}\hat{l}_6'\begin{bmatrix}2L+1\\2l_2'\end{bmatrix}^{1/2}k^{L-l_2'}C^{J}_{-J_z\,m_2m_5'}{}^{t_2\;l_5'}\begin{Bmatrix}l_5' & L & t_1\\ S & t_2 & J\end{Bmatrix}$$

$$\times\Bigg\{(-1)^{L+t_1+l_5'}I'_{C_1}(l_2',l_6')C_{0\,0\,0}^{l_2'l_6't_1}[Y^{L-l_2'}(\hat{\mathbf{k}}')\otimes Y^{l_6'}(\hat{\mathbf{R}}')]_{m_5'}^{l_5'}\begin{Bmatrix}L & L-l_2' & l_2'\\ l_6' & t_1 & l_5'\end{Bmatrix}$$

$$-\frac{8\sqrt{3\pi}}{9p_0^2}|\mathbf{q}'-\mathbf{k}|I'_{C_2}(l_2',l_6')$$

$$\times\sum_{l_3',l_4'}\hat{l}_3'\hat{l}_4'C_{0\,0\,0}^{1\,l_2'l_3'}C_{0\,0\,0}^{l_3'l_6't_1}\{[Y^{L-l_2'}(\hat{\mathbf{k}}')\otimes Y^{l_6'}(\hat{\mathbf{R}}')]^{l_4'}\otimes\widehat{Y^1(\mathbf{q}'-\mathbf{k})}\}_{m_5'}^{l_5'}\begin{Bmatrix}L & t_1 & l_5'\\ L-l_2' & l_6' & l_4'\\ l_2' & l_3' & 1\end{Bmatrix}\Bigg\}, \tag{B19}$$

where

$$\mathbf{R}'\equiv\mathbf{k}+\mathbf{k}'-\mathbf{q}', \tag{B20}$$

$$I_C(l_1,l_2,l_6)\equiv\int_0^\infty dq\frac{q^{l_1+l_2+4}}{D_\pi(q,\omega_C)}F_C^\pi(q)e^{-q^2/p_0^2}i_{l_6}(qR'/p_0^2), \tag{B21}$$

$$I'_{C_1}(l_2',l_6')$$

$$\equiv\int_0^\infty dq\frac{q^{l_2'+4}[(2/3p_0^2)(q^2+|\mathbf{q}'-\mathbf{k}'|^2)-1]}{D_\pi(q,\omega_C)}F_C^\pi(q)e^{-q^2/p_0^2}i_{l_6'}(qR'/p_0^2), \tag{B22}$$

$$I'_{C_2}(l_2',l_6')\equiv\int_0^\infty dq\frac{q^{l_2'+5}}{D_\pi(q,\omega_C)}F_C^\pi(q)e^{-q^2/p_0^2}i_{l_6'}(qR'/p_0^2). \tag{B23}$$

As in the case of $\tilde{B}_1$, these integrals can be evaluated numerically using Gauss-Legendre quadrature. The quantity $C_{1b}(t_1,t_2,m_2)$, which is independent of the detailed nuclear structure, is given by

$$C_{1b}(t_1,t_2,m_2)=16\pi\sqrt{2}q'\hat{S}\sum_{m_1}\sum_{S''}(-1)^{S+S''}\hat{S}''^2\hat{t}_2^2C_{000}^{11t_1}C_{m_1\,m_2S_z'}^{1\;\;t_2\;\;S'}Y_{m_1}^1(\hat{\mathbf{q}}')\begin{Bmatrix}1 & S & S''\\ \frac{1}{2} & \frac{1}{2} & \frac{1}{2}\end{Bmatrix}\begin{Bmatrix}1 & S & S''\\ t_2 & 1 & t_1\end{Bmatrix}\begin{Bmatrix}1 & S'' & t_1\\ \frac{1}{2} & \frac{1}{2} & S'\\ \frac{3}{2} & \frac{1}{2} & 1\end{Bmatrix}. \tag{B24}$$

4. Amplitude $\tilde{D}_1$

In analogy with the previous amplitudes discussed in this Appendix, we write the reduced amplitude $\tilde{D}_1$ as the product of three factors,

$$\tilde{D}_1=D_1^ID_{1a}D_{1b}\{Y^L(\hat{q}_A)\otimes[Y^1(\hat{\mathbf{q}}_D)\otimes Y^1(\hat{\mathbf{q}}')]^S\}_{J_z}^J, \tag{B25}$$

where $\mathbf{q}_A$ is defined in Eq. (B1), and

$$\mathbf{q}_D=\mathbf{k}-\mathbf{k}'. \tag{B26}$$

The isospin factor for amplitude $\tilde{D}_1$, D_1^I, is given in Eq. (A6). D_{1a} and D_{1b} refer to

$$D_{1a}=\sqrt{4\pi}(i)^L(-1)^{l_h+L+J+J_z}\frac{f_{\pi NN}f_{\pi N\Delta}^2}{m_\pi^3}\frac{\hat{l}_p\hat{l}_h}{\hat{L}}C_{0\,0\,0}^{l_p\,l_h\,L}$$

$$\times F_D^\pi(q_D)\frac{A_{l_p',l_h,L}^{n,n'}(q_A)}{D_\pi(q_D,\omega_D)D_\Delta(q_D^\Delta,\omega_D^\Delta)} \tag{B27}$$

and

$$D_{1b}=2(8\pi/3)^{3/2}q'q_D^2(-1)^{S+1}Y_{S_z'}^1(\hat{\mathbf{q}}_D)$$

$$\times\begin{Bmatrix}1 & 1 & S\\ \frac{1}{2} & \frac{1}{2} & \frac{3}{2}\end{Bmatrix}\delta_{S',1}, \tag{B28}$$

where $A_{l_p',l_h,L}^{n,n'}$ is defined in Eq (B7).

APPENDIX C: PREEMISSION AMPLITUDES $\tilde{A}_2$, $\tilde{B}_2$, $\tilde{C}_2$, AND $\tilde{D}_2$ IN PLANE-WAVE APPROXIMATION

1. Amplitude $\tilde{A}_2$

In principle, we should calculate both the preemission and postemission amplitudes for the $(N,N'\pi)$ reaction. However, as we shall see the preemission amplitudes for $(p,p'\pi^+)$ are negligible for energies appropriate to this calculation. As a result it is sufficient to evaluate the preemission amplitudes only in plane-wave approximation, where they can be compared with postemission amplitudes listed in Appendix B.

We define the preemission amplitudes analogous to the postemission amplitudes, breaking each amplitude up into a produce of isospin, spin, and angular momentum factors. We use the same form as in Appendix B for the preemission amplitudes $\tilde{A}_2$, $\tilde{B}_2$, $\tilde{C}_2$, and $\tilde{D}_2$. For example, we write the first such term as

$$\tilde{A}_2 = A_2^I A_2^a A_2^b \ . \tag{C1}$$

The term A_2^a can be obtained from A_1^a of Eq. (B5) with the substitutions $q_A^\Delta \rightarrow |\mathbf{k}-\mathbf{q}'|$ and $\omega_A^\Delta \rightarrow E - E_\pi$. All such preemission terms can be obtained from the analogous postemission amplitudes with the same substitution.

The corresponding isospin factor is

$$A_2^I = 2C^{1/2\,1\,3/2}_{t_{z_f}\,T_z t_{z_\Delta}} C^{3/2\,1\,1/2}_{t_{z_\Delta}\,\lambda' t_{z_i}} (\hat{\phi}'\dagger)_{\lambda'} \delta_{T,1} \ , \tag{C2}$$

with the value of $(\sqrt{2}/3)\delta_{T,1}$ for the $(p,p'\pi^+)$ reaction. Also,

$$A_2^b = -2(8\pi/3)^{3/2}(-1)^{S'} q' q_A^2 [Y^1(\hat{\mathbf{q}}') \otimes Y^1(\hat{\mathbf{q}}_A)]^{S'}_{S_z'} \times \begin{Bmatrix} 1 & 1 & S' \\ \frac{1}{2} & \frac{1}{2} & \frac{3}{2} \end{Bmatrix} \delta_{S,1} \ . \tag{C3}$$

2. Amplitude $\tilde{B}_2$

From the discussion in the previous subsection, we need only give formulas for the isospin and spin coefficient for this term. The isospin factor, B_2^I, is given by

$$B_1^I = 4\sqrt{2}(-1)^{t_{z_i}+T_z+1/2} C^{1/2\,1/2\,1}_{t_{z_i}\,-t_{z_f}\,-T_z'} C^{1\,1\,T}_{T_z'\,\lambda'\,-T_z} \times \begin{Bmatrix} \frac{1}{2} & 1 & \frac{3}{2} \\ 1 & \frac{1}{2} & T \end{Bmatrix} (\hat{\phi}'\dagger)_{\lambda'} \ , \tag{C4}$$

and has the value of $\sqrt{2}/3$ for $(p,p'\pi^+)$.

The preemission expression for B_{1b} is given by (the only difference from the postemission amplitude is a change in phase)

$$B_{1b}(t_1,t_2,m_2) = 16\pi\sqrt{2} q' \hat{S} \sum_{m_1} \sum_{S''} (-1)^{S'+S''+1} \hat{S}'' \hat{t}_2^2 C^{1\,1\,t_1}_{0\,0\,0} C^{1\ t_2\ S'}_{m_1\,m_2\,S_z'} Y^1_{m_1}(\hat{\mathbf{q}}') \begin{Bmatrix} 1 & S & S'' \\ \frac{1}{2} & \frac{1}{2} & \frac{1}{2} \end{Bmatrix} \begin{Bmatrix} 1 & S & S'' \\ t_2 & 1 & t_1 \end{Bmatrix} \begin{Bmatrix} 1 & S'' & t_2 \\ \frac{1}{2} & \frac{1}{2} & S' \\ \frac{3}{2} & \frac{1}{2} & 1 \end{Bmatrix} , \tag{C5}$$

with

$$q_B^\Delta \approx q' \ , \quad \omega_B^\Delta \approx m_N - E_\pi \ . \tag{C6}$$

3. Amplitude $\tilde{C}_2$

The isospin factor for the preemission amplitude $\tilde{C}_2$ reduces to

$$C_2^I = 2\sqrt{6}(-1)^{T_z} \hat{T} C^{3/2\ T\ 1/2}_{-t_{z_\Delta}\ T_z\ -t_{z_f}} C^{3/2\,1\,1/2}_{t_{z_\Delta}\,\lambda' t_{z_i}} \times \begin{Bmatrix} \frac{3}{2} & \frac{1}{2} & 1 \\ \frac{1}{2} & \frac{1}{2} & T \end{Bmatrix} (\hat{\phi}'\dagger)_{\lambda'} \ , \tag{C7}$$

and has the value of $\sqrt{2}/3$ for $(p,p'\pi^+)$. The spin factor C_{1b} has the form

$$C_{1b}(t_1,t_2,m_2) = 16\pi\sqrt{2} q' \hat{S} \sum_{m_1} (-1)^{S+1} \hat{t}_2^2 C^{1\,1\,t_1}_{0\,0\,0} C^{1\ t_2\ S'}_{m_1\,m_1\,S_z'} Y^1_{m_1}(\hat{\mathbf{q}}') \times \begin{Bmatrix} 1 & t_2 & S' \\ \frac{1}{2} & \frac{1}{2} & \frac{3}{2} \end{Bmatrix} \begin{Bmatrix} 1 & 1 & t_1 \\ \frac{1}{2} & \frac{1}{2} & S \\ \frac{3}{2} & \frac{1}{2} & t_2 \end{Bmatrix} \tag{C8}$$

with

$$q_C^\Delta = |\mathbf{k}-\mathbf{q}'| \ , \quad \omega_C^\Delta = E - E_\pi \ . \tag{C9}$$

4. Amplitude $\tilde{D}_2$

The isospin factor for the preemission amplitude $\tilde{D}_2$ is

$$D_2^I = 4\sqrt{2}(-1)^{\lambda'-t_{z_f}+1/2} C^{1/2\,1/2\,1}_{t_{z_i}\,-t_{z_f}\,\lambda} C^{1\,1\,T}_{\lambda'\,-\lambda\,-T_z} \times \begin{Bmatrix} \frac{1}{2} & 1 & \frac{3}{2} \\ 1 & \frac{1}{2} & T \end{Bmatrix} (\hat{\phi}'\dagger)_{\lambda'} \ , \tag{C10}$$

and has the value of $-\sqrt{2}/3$ for $(p,p'\pi^+)$. The preemission expression for D_{1b} is

$$D_{1b} = -2 \left[\frac{8\pi}{3} \right]^{3/2} q' q_D^2 Y^1_{S_z'}(\hat{\mathbf{q}}_D) \begin{Bmatrix} 1 & 1 & S \\ \frac{1}{2} & \frac{1}{2} & \frac{3}{2} \end{Bmatrix} \delta_{S',1} \ , \tag{C11}$$

with

$$q_D^\Delta \approx q' \ , \quad \omega_D^\Delta \approx m_N - E_\pi \ . \tag{C12}$$

[1] *Proceedings of the Conference on Pion Production and Absorption in Nuclei,* AIP Conf. Proc. No. 79, edited by R. D. Bent (AIP, New York, 1982).
[2] B. Hoistad, Adv. Nucl. Phys. **11**, 135 (1979); D. F. Measday and G. A. Miller, Annu. Rev. Nucl. Part. Sci. **29**, 121 (1979); H. W. Fearing, Prog. Part. Nucl. Phys. **7**, 113 (1981); G.E. Walker, Comm. Nucl Part. Phys. A **11**, 169 (1983); D. A. Ashery and J. P. Schiffer, Annu. Rev. Nucl. Part. Sci. **36**, 207 (1986).
[3] H. S. Sherif, S. W. Leung, A. W. Thomas, and G. Brookfield, Phys. Lett. **83B**, 293 (1979).
[4] W. W. Jacobs *et al.*, Phys. Rev. Lett. **49**, 855 (1982); S. E. Vigdor *et al.*, *ibid.* **49**, 1314 (1982); Z-J. Cao, R. D. Bent, H. A. Nann, and T. E. Ward, Phys. Rev. C **35**, 625 (1987); T. G Throwe *et al.*, *ibid.* **35**, 1083 (1987); E. Korkmaz *et al.*, Phys. Rev. Lett. **58**, 104 (1987).
[5] Z. Grossman, F. Lenz, and M. P. Locher, Ann. Phys. (N.Y.) **84**, 348 (1974).
[6] L. S. Kisslinger and W. L. Wang, Phys. Rev. Lett. **30**, 1071 (1973); Ann. Phys. (N.Y.) **99**, 374 (1976).
[7] W.Weise, Nucl. Phys. **A278**, 402 (1977); E. Oset and W. Weise, Phys. Lett. **B77**, 159 (1978); Nucl. Phys. **A319**, 477 (1979); **A322**, 365 (1979).
[8] M. Hirata, J. H. Koch, F. Lenz, and E. J. Moniz, Phys. Lett. **70B**, 281 (1977); M. Hirata, F. Lenz, and K. Yazaki, Ann. Phys. (N.Y.) **108**, 116 (1977); M. Hirata, J. H. Koch, F. Lenz, and E. J. Moniz, *ibid.* **120**, 205 (1979); J. H. Koch and E. J. Moniz, Phys. Rev. C **20**, 235 (1979).
[9] Y. Horikawa, M. Thies, and F. Lenz, Nucl. Phys. **A345**, 386 (1980); F. Lenz, E. J. Moniz, and K. Yazaki, Ann. Phys. (N.Y.) **129**, 84 (1980); F. Lenz, M. Thies, and Y. Horikawa, *ibid.* **140**, 266 (1982); M. Thies, Nucl. Phys. **A382**, 434 (1982).
[10] K. Klingenbeck, M. Dillig, and M. G. Huber, Phys. Rev. Lett. **41**, 387 (1978).
[11] C. L. Morris *et al.*, Phys. Lett. **108B**, 172 (1982); M. Baumgartner *et al.*, *ibid.* **112B**, 35 (1982); Nucl. Phys. **A399**, 451 (1983).
[12] J. H. Koch and E. J. Moniz, Phys. Rev. C **27**, 751 (1983); M. Hirata, F. Lenz, and M. Thies, *ibid.* **28**, 875 (1983); T. Takaki, T. Suzuki, and J. H. Koch, Nucl. Phys. **A443**, 570 (1985); T. Takaki and M. Thies, Phys. Rev. C **38**, 2230 (1988).
[13] D. Contardo *et al.*, Phys. Lett. **168B**, 331 (1986); C. Ellegaard, Phys. Rev. Lett. **59**, 974 (1987); M. Roy-Stephan, Nucl. Phys. **A488**, 187c (1988); C. Gaarde, in *Proceedings of the Conference on Spin and Isospin in Nuclear Interactions,* edited by S. W. Wissink, C. D. Goodman, and G. E. Walker (Plenum, New York, 1991), p. 295.
[14] B. K. Jain, J. T. Londergan, and G. E. Walker, Phys. Rev. C **37**, 1564 (1988).
[15] G. E. Brown and W. Weise, Phys. Rep. **27**, 1 (1976).
[16] E. Oset, H. Toki, and W. Weise, Phys. Rep. **83**, 282 (1982).
[17] Rami Mehrem, Ph.D. thesis, Indiana University 1992 (unpublished).
[18] D. Robson and R. D. Koshel, Phys. Rev. C **6**, 1125 (1972); L. A. Charlton, *ibid.* **8**, 146 (1973).
[19] Robert Bent (private communication).
[20] Edward Siciliano (private communication).
[21] K. Stricker, H. McManus, and J. A. Carr, Phys. Rev. C **19**, 929 (1979).
[22] M. Ericson and T. E. O. Ericson, Ann. Phys. **36**, 323 (1966).
[23] T. W. Donnelly and G. E. Walker, Ann. Phys. **60**, 209 (1970).
[24] R. Mehrem, J. T. Londergan, and M. H. Macfarlane, J. Phys. A **24**, 1435 (1991).
[25] A. B. Migdal, Rev. Mod. Phys. **50**, 107 (1978).
[26] J. Meyer-ter-Vehn, Z. Phys. A **287**, 241 (1978); Phys. Rep. **74**, 323 (1981).
[27] H. Toki and W. Weise, Z. Phys. A **292**, 389 (1979); **295**, 187 (1980).
[28] J. Speth, V. Klemt, J. Wambach, and G. E. Brown, Nucl. Phys. **A343**, 382 (1980).
[29] A. Fetter and J. D. Walecka, *Quantum Theory of Many-Particle Systems* (McGraw Hill, New York, 1971).
[30] T. deForest, Jr. and J. D. Walecka, Adv. Phys. **15**, 1 (1966).
[31] E. R. Siciliano and G. E. Walker, Phys. Rev. C **23**, 2661 (1981).
[32] *Handbook of Mathematical Functions,* edited by M. Abramowitz and I. A. Stegun (National Bureau of Standards, 1964).